FLUORESCENCE SPECTROSCOPIC AND MOLECULAR MODELLING STUDIES ON THE MOLECULAR INTERACTION MECHANISM OF BROMODEOXYURIDINE WITH HUMAN SERUM ALBUMIN

AMIRA ADLIN BINTI ROSLAN

FACULTY OF SCIENCE
UNIVERSITY OF MALAYA
KUALA LUMPUR

2021

FLUORESCENCE SPECTROSCOPIC AND MOLECULAR MODELLING STUDIES ON THE MOLECULAR INTERACTION MECHANISM OF BROMODEOXYURIDINE WITH HUMAN SERUM ALBUMIN

AMIRA ADLIN BINTI ROSLAN

DISSERTATION SUBMITTED IN FULFILMENT OF THE REQUIREMENTS FOR THE DEGREE OF MASTER OF SCIENCE

**INSTITUTE OF BIOLOGICAL SCIENCES
FACULTY OF SCIENCE
UNIVERSITI MALAYA
KUALA LUMPUR**

2021

UNIVERSITI MALAYA
ORIGINAL LITERARY WORK DECLARATION

Name of Candidate: **AMIRA ADLIN BT ROSLAN** ———

Matric No: **17013622/1 (SMA 180001)**

Name of Degree: **MASTER OF SCIENCE**

Title of Dissertation:

FLUORESCENCE SPECTROSCOPIC AND MOLECULAR MODELLING STUDIES ON THE MOLECULAR INTERACTION MECHANISM OF BROMODEOXYURIDINE WITH HUMAN SERUM ALBUMIN

Field of Study: **BIOCHEMISTRY**

I do solemnly and sincerely declare that:

(1)   I am the sole author/writer of this Work;

(2)   This Work is original;

(3)   Any use of any work in which copyright exists was done by way of fair dealing and for permitted purposes and any excerpt or extract from, or reference to or reproduction of any copyright work has been disclosed expressly and sufficiently and the title of the Work and its authorship have been acknowledged in this Work;

(4)   I do not have any actual knowledge nor do I ought reasonably to know that the making of this work constitutes an infringement of any copyright work;

(5)   I hereby assign all and every rights in the copyright to this Work to the University of Malaya ("UM"), who henceforth shall be owner of the copyright in this Work and that any reproduction or use in any form or by any means whatsoever is prohibited without the written consent of UM having been first had and obtained;

(6)   I am fully aware that if in the course of making this Work I have infringed any copyright whether intentionally or otherwise, I may be subject to legal action or any other action as may be determined by UM.

Candidate's Signature   Date: December 16, 2020

Subscribed and solemnly declared before,

Witness's Signature   Date: Dec. 22, 2020
Name:
Designation:

Witness's Signature   Date: Dec. 30, 2020
Name:
Designation:

FLUORESCENCE SPECTROSCOPIC AND MOLECULAR MODELLING STUDIES ON THE MOLECULAR INTERACTION MECHANISM OF BROMODEOXYURIDINE WITH HUMAN SERUM ALBUMIN

ABSTRACT

The interaction of a nucleoside analogue, bromodeoxyuridine (BrdU) with human serum albumin (HSA) was studied to investigate the binding phenomenon and analyze the protein conformation upon BrdU binding. Multiple spectroscopic techniques, viz. intrinsic and three-dimensional (3-D) fluorescence, ultraviolet-visible (UV-Vis) absorption and circular dichroism (CD) spectroscopy along with molecular docking were used. A decrease in the Stern-Volmer constant (K_{sv}) with the increase in temperature suggested BrdU-induced quenching of protein fluorescence as static quenching and thus implied BrdU−HSA complex formation. This was also supported by UV-Vis absorption spectral results, showing hyperchromism in the absorption spectrum of HSA upon BrdU addition. Intermediate binding affinity between BrdU and HSA was evident from the K_a values (2.49–3.97 $\times$ 10^4 M^{-1}), while BrdU−HSA complex formation was driven by hydrophobic and van der Waals interactions along with hydrogen bonds, as revealed by thermodynamic data (ΔS = +28.48 J mol^{-1} K^{-1}; ΔH = −17.16 kJ mol^{-1}). The feasibility of the binding reaction was confirmed from the negative sign of ΔG values. The binding reaction was found to be exothermic in nature, as disclosed by the negative ΔH value, which also supported the decrease in the K_a value with increasing temperature. Minor changes occurred in both secondary and tertiary structures as well as in the fluorophores' microenvironment of HSA, as recognized from the CD spectral results in the far-UV and the near-UV regions and 3-D fluorescence spectra, respectively. Use of site markers (warfarin and indomethacin for the site I; diazepam for site II), as well as docking results, suggested BrdU binding to

both site I (more preferred) and site II, located in subdomains IIA and IIIA, respectively, of HSA. A small but significant influence of several metal ions on the binding reaction between BrdU and HSA was also noticed.

Keywords: bromodeoxyuridine, human serum albumin, drug-protein interaction, fluorescence quenching, molecular modelling

KAJIAN SPEKTROSKOPI PENDARFLUOR DAN PERMODELAN MOLEKUL TERHADAP MEKANISME INTERAKSI MOLEKUL BROMODEOXYURIDINE DENGAN ALBUMIN SERUM MANUSIA

ABSTRAK

Interaksi di antara analog nukleosida, bromodeoxyuridine (BrdU) dengan manusia serum albumin (HSA) telah dikaji untuk menyelidik pengikatan BrdU terhadap fenomena pengikatan dan menganalisis pembentukan protein. Pelbagai kaedah spektroskopik seperti intrinsik dan tiga-dimensi (3-D) pendarfluor, penyerapan ultralembayung jelas (UV-vis) dan dikroisme bulatan (CD) spektroskopik serta dok molekular telah digunakan. Penurunan nilai konstan Stern-Volmer (K_{sv}) dengan penaikan suhu mencadangkan pelindapkejutan protein bersama BrdU sebagai pelindapkejutan statik dan seterusnya pembentukan kompleks BrdU−HSA. Hal ini juga disokong oleh hasil penyerapan ultralembayung jelas UV-Vis yang menunjukkan hiperkroisme pada spektrum penyerapan HSA semasa penambahan BrdU. Kesederhanaan afiniti pengikatan di antara BrdU−HSA merupakan bukti daripada nilai-nilai K_a ($2.49 − 3.97 \times 10^4$ M^{-1}), sementara pembetukan kompleks BrdU−HSA adalah didorong oleh daya hidrofobik dan van der Waals serta ikatan hidrogen, seperti yang dapat dilihat daripada data termodinamik ($\Delta S = +28.48$ J mol^{-1} K^{-1}; $\Delta H = −17.16$ kJ mol^{-1}). Kemungkinan reaksi pengikatan telah disahkan oleh nilai-nilai negatif ΔG. Reaksi pengikatan adalah eksotermik semula jadi seperti yang didedahkan oleh nilai negatif ΔH, yang juga menyokong penurunan nilai K_a dengan penaikan suhu. Perubahan kecil yang telah berlaku dalam struktur sekunder dan tertier serta persekitaran mikro pendarfluor HSA, masing-masing dapat dilihat daripada hasil kajian oleh spektra CD ultralembayung jauh dan dekat dan 3-D spektra pendarfluor. Penggunaan penanda tapak (warfarin dan indometasin untuk tapak I; diazepam untuk tapak II), serta hasil dok, mencadangkan BrdU mengikat kepada tapak I (lebih diutamakan) dan tapak II, di mana

masing-masing terletak dalam subdomain IIA dan IIIA HSA. Pengaruh yang kecil tetapi signifikan oleh ion logam juga dapat dilihat pada reaksi pengikatan antara BrdU dan HSA.

Kata kunci: bromodeoxyuridine, albumin serum manusia, interaksi ligan-protein, pelindapkejutan kependarfluoran, permodelan molekul

ACKNOWLEDGEMENTS

This dissertation becomes a reality with the kind support and help of many individuals. I would like to express absolute gratitude to all of them.

Foremost, I want to offer this endeavour to ALLAH SWT for the wisdom He bestowed upon me, the strength and good health in order to finish this research.

My deep appreciation goes first to my supervisors, Professor Dr. Saad Tayyab and Associate Professor Dr. Saharuddin bin Mohamad, who expertly guided me throughout my research journey. It has been a marvellous opportunity to work under their supervision.

Dr Md. Zahirul Kabir, Dr Nurul Iman Ahamed Kameel, Dr Foo Yiing Yee and Sam Si Enn are sincerely appreciated for their support and guidance during the experimental work. I am also felt blessed to have lab mates and seniors, who were very supportive and were always be there whenever I needed them.

I would like to extend my sincere thanks towards my family for their endless encouragement, advice and prayers for me to complete this dissertation.

Amira Adlin Binti Roslan

May 2020

TABLE OF CONTENTS

LIST OF FIGURES

LIST OF TABLES

LIST OF ABBREVIATIONS AND SYMBOLS

Ala	:	Alanine
Arg	:	Arginine
Å	:	Angstrom
a.u.	:	Arbitrary unit
$BaCl_2$	:	Barium chloride
BrdU	:	Bromodeoxyuridine
$CaCl_2$	:	Calcium chloride
CD	:	Circular dichroism
cm	:	Centimetre
$CuCl_2$	:	Copper (II) chloride
Cys	:	Cysteine
Da	:	Dalton
dAK	:	Deoxyadenosine kinase
dCK	:	Deoxycytidine kinase
dGK	:	Deoxyguanosine kinase
dL	:	Decilitre
DMSO	:	Dimethyl sulphoxide
DNA	:	Deoxyribonucleic acid
DZM	:	Diazepam
3-D	:	Three-dimensional
e.g.	:	Latin phrase *exempli gratia* (for example)
ε_m	:	Molar extinction coefficient
FI	:	Fluorescence intensity
g	:	Gram
Glu	:	Glutamic acid

h	:	Hour
His	:	Histidine
HSA	:	Human serum albumin
i.e.	:	Latin phrase *id est* (that is)
IDN	:	Indomethacin
Ile	:	Isoleucine
J	:	Joules
K	:	Kelvin
K_a	:	Association / binding constant
KCl	:	Potassium chloride
kJ	:	Kilojoules
k_q	:	Bimolecular quenching rate constant
K_{sv}	:	Stern-Volmer constant
Leu	:	Leucine
Lys	:	Lysine
M	:	Molar
mdeg	:	Millidegree
mg	:	Milligram
$MgCl_2$	:	Magnesium chloride
min	:	Minute
mL	:	Millilitre
$MnCl_2$	:	Manganese (II) chloride
NA	:	Nucleoside analogue
nm	:	Nanometre
P	:	Phosphate
PB	:	Phosphate buffer

PDB	:	Protein Data Bank
PVDF	:	Polyvinylidene fluoride
RNA	:	Ribonucleic acid
s	:	Second
S	:	Svedberg unit
SD	:	Standard deviation
Ser	:	Serine
T	:	Temperature
TK1	:	Tyrosine kinase 1
TK2	:	Tyrosine kinase 2
Trp	:	Tryptophan
Tyr	:	Tyrosine
μm	:	Micrometer
UV	:	Ultraviolet
UV-Vis	:	Ultraviolet-visible
V	:	Voltage
Val	:	Valine
viz.	:	Latin phrase *videlicet* (that is to say)
WFN	:	Warfarin
μL	:	Microliter
μM	:	Micromolar
~	:	Approximate
λ_{em}	:	Emission wavelength
λ_{ex}	:	Excitation wavelength
ΔG	:	Gibbs free energy change
ΔH	:	Enthalpy change

ΔS :   Entropy change

$>$:   Greater than

CHAPTER 1: INTRODUCTION

The nucleoside analogues deter the cell cycle by impairment in the DNA / RNA synthesis (Wigler & Lozzio, 1972; Jordheim et al., 2013). Bromodeoxyuridine (BrdU, Fig. 2.4B), a nucleoside analogue of thymidine is commonly used in studying cell cycle kinetics, DNA replication as well as in the assessment of cell proliferation of pathological cells or tissues under different conditions (Galmarini, Mackey & Dumontet, 2002; Eyer et al., 2018). BrdU treatment of cancer cells, followed by immunohistochemical detection with anti-BrdU antibodies has been found successful in detecting proliferating cancer cells during S-phase in DNA replication (Nakamura et al., 1991). In comparison to thymidine, BrdU has shown better incorporation into DNA through replication during S-phase due to larger size of halogen attached to it and its capacity to readily cross the blood brain barrier (Lengronne et al., 2001; Levkoff et al., 2008). Although several studies have been made to investigate the BrdU effectiveness and functions in human cells (Hill, Tsuboi & Baserg, 1974; Kuhn & Cooper-Kuhn, 2007), its transport in human blood circulation is still remained to be investigated.

The delivery of numerous endogenous and exogenous compounds including drugs to their target organs / tissues in human blood circulation is mainly assisted by human serum albumin (HSA), the major transport protein in blood plasma (Kragh-Hansen, Chuan & Otagiri, 2002; Mothi et al., 2005). Interaction of the drug with the plasma protein may lead to alteration in the pharmacokinetics and pharmacodynamics of the drug (Hu et al., 2010). Human serum albumin is a single polypeptide chain, comprised of three similar domains (I, II and III), with each containing two subdomains, A and B. It consists of two high affinity binding sites; Sudlow's sites I and II, located in subdomains IIA and IIIA, respectively, which underlies its importance in interacting with many organic and inorganic molecules (Sudlow, Birkett & Wade, 1975; El Kadi et al., 2006; Shahabadi et al., 2017). Therefore, detailed information about the interaction

between BrdU and HSA is required to understand the binding characteristics as well as to study the effect of BrdU−HSA complexation on protein stability and structure. Hence, both experimental and computational approaches were used in this study.

Problem Statement

Is BrdU transported by human serum albumin in human circulation? If yes, what are the binding characteristics of BrdU−HSA interaction and how this binding affects protein structure and stability?

Objectives of the study

1. To characterize the binding affinity and binding forces involved in the interaction between BrdU and HSA.

2. To investigate the influence of BrdU binding on the secondary and tertiary structures of HSA as well as microenvironmental changes around protein fluorophores along with protein's thermal stability.

3. To characterize the BrdU binding site on HSA using molecular modelling studies.

4. To evaluate the influence of metal ions on BrdU–HSA binding affinity.

CHAPTER 2: LITERATURE REVIEW

2.1 Cancer

Cancer incidence and mortality are hastily growing worldwide. In 2018, the number of new cancer cases and deaths had risen to 18.1 and 9.6 million, respectively (Siegel, Miller & Jemal, 2018). Apart from being the most prevalent diagnosed cancer with 11.6 % of the total incidences, lung cancer is also said to be the leading cause of cancer annihilation, contributing 18.4 % of the total cancer deaths (Barta, Powell & Wisnivesky, 2019). The proportion of the cancer prevalence is closely followed by female breast cancer (11.6 %), colorectum cancer (10.2 %) and prostate cancer (7.1 %), while colorectum cancer (9.2 %), stomach cancer (8.2 %) and liver cancer (8.2 %) are acknowledged for mortality rate (Barta, Powell & Wisnivesky, 2019). While lung cancer is the main determinant of death rates in male population (Torre et al., 2016; Barta et al., 2019), breast cancer has frequent occurrence and mortality among females (Mingqiang et al., 2019). The most prevailing factors contributing to cancer genesis and development are biological, environmental exposure, occupational and lifestyle-related factors (Wang et al., 2014; Bayo et al., 2019). Therefore, these influences may alter cell cycle leading to cancer cell proliferation (Park et al., 2011). Hence, it is vital to identify molecular and cellular targets that can inhibit cancer cell proliferation and therefore, are liable in managing and preventing cancer incidence and mortality. Herein, nucleoside analogues can be the quintessential targets for the therapeutic advancements in cancer management.

2.2 Nucleoside analogues as chemotherapeutic agents

Nucleoside analogues (NAs) are synthetic endogenous compounds, that are chemically modified to mimic the physiological aspects of their counterparts (Jordheim et al., 2013; Eyer et al., 2018). The structure of these compounds includes a nitrogenous base analogue linked to a sugar unit (Thomson & Lamont, 2019). On the other hand,

they are chemically diverse based on the modifications such as halogenation, azotation etc. (Jordheim et al., 2013; Ismail et al., 2020). These analogues are pivotal components of anticancer, antiviral and immunosuppressant drugs (Perigaud, Gosselin & Imbach, 1992; Diab et al., 2007). These compounds inhibit DNA synthesis by their incorporation into the DNA and RNA growing chains. They interfere with various enzymatic activities in the nucleic acids' synthesis and thus results in the induction of apoptotic cell death (Galmarini et al., 2002; Ruiz-Magana et al., 2016; Yasui et al., 2019).

Figure 2.1 shows the comparison between the structures of several NAs and their counterparts (purine and pyrimidine), that are widely used in chemotherapy. Cladribine, abacavir, fludarabine and clofarabine are among purine NAs, that are mainly used against hematological malignancies (Barua et al., 2019; Barre et al., 2019) such as lymphatic leukemia and HIV infection (Szymczyk et al., 2019). Pyrimidine NAs include gemcitabine, lamivudine, decitabine and cytarabine, which are also practiced in treating hematological malignancies as well as some cancerous diseases such as breast, pancreatic and ovarian cancers (Lapponi et al., 2016; Mottini et al., 2019).

Generally, these NAs are administered intravenously in different dosage forms, *e.g.* gemcitabine (1000 mg / m^2) and cisplatin (100 mg / m^2) (Rades et al., 2016; Kim et al., 2018). Endogenous nucleosides and NAs generally exhibit similar metabolic pathways, as shown in Figure 2.2 (Jordheim et al., 2013). Both are transported into the membrane either via diffusion or through nucleoside transporters (Cano-Soldado & Pastor-Anglada, 2011; Minuesa et al., 2011). Penetration of these compounds into the cells, subsequently leads to the activation steps, involving the formation of active phosphate derivatives (Lapponi et al., 2016; Tsesmetzis et al., 2018). Figure 2.3 demonstrates the catalytic action of nucleoside kinase, nucleoside monophosphate kinase, nucleoside diphosphate kinase and 3-phosphoglycerate kinase that take place in the phosphorylation of non-natural nucleosides (Rompay, Johansson & Karlsson, 2000).
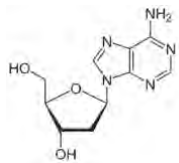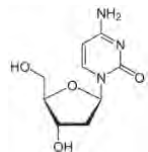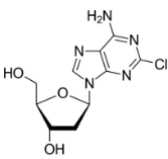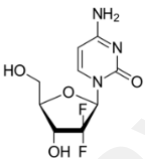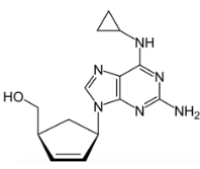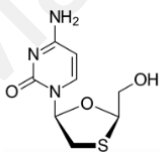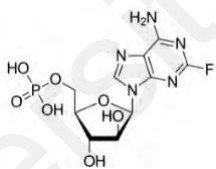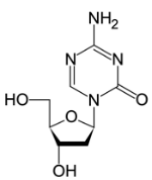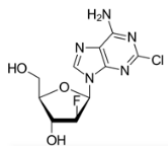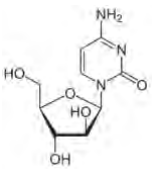
Figure 2.1: Chemical structures of FDA-approved nucleoside analogues and their counterparts, deoxyadenosine and deoxycytidine, that are widely used in chemotherapy.
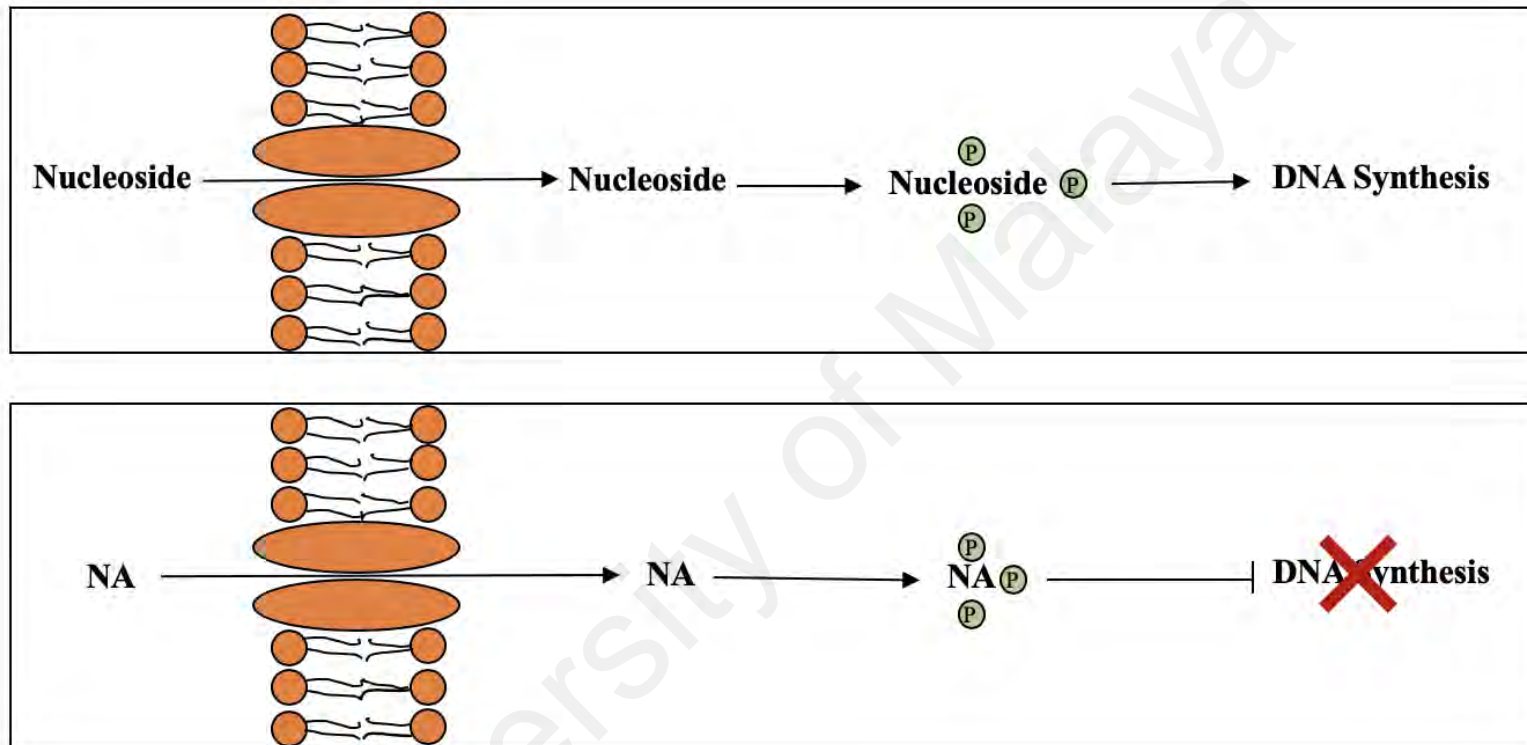
Figure 2.2: Schematic diagram showing the comparison of metabolic pathways between endogenous nucleoside and nucleoside analogue (NA).
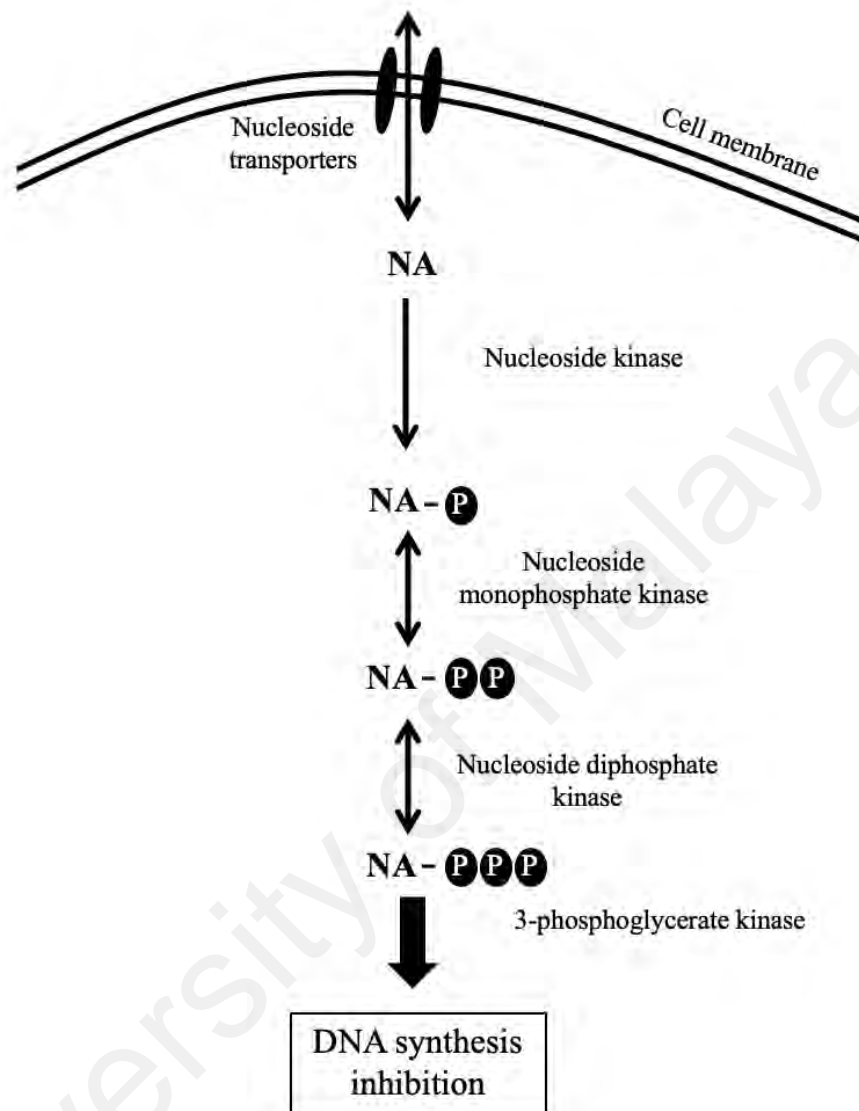
Figure 2.3: Schematic diagram showing the mechanism of nucleoside analogue in the cell.

The examples of human deoxyribonucleoside kinases are thymidine kinase (TK1 and TK2), deoxycytidine kinase (dCk), deoxyadenosine kinase (dAk) and deoxyguanosine kinase (dGk). While the mechanism of action of naturally occurring nucleosides contributes to the synthesis of DNA, opposite effect is noticed from the mechanism of action of NAs. The active form of NAs shows cytotoxic activity by disrupting the DNA synthesis through inhibition of the extracellular enzymes such as DNA polymerases and ribonucleotide reductases (Galmarini et al., 2002). This leads to the accumulation of di- and triphosphorylated NAs in cancer or virus infected-cells, which consequently block the synthesis of DNA (Fung et al., 2011).

Several studies have reported that NA molecules are advantageous in terms of their greater *in vitro* stability, overcoming drug resistance, sustained drug release and prolonged biological half-life (Moog et al., 2002; Celano et al., 2004; Port et al., 2006). Table 2.1 shows several NAs along with therapeutic interests for different cancers. Therefore, NAs have been extensively used in treating various types of cancers, as they are highly stable, efficient as well as able to incorporate directly into the newly-synthesized DNA, thus leading to the termination of chain elongation, accumulation of mutation and causing apoptotic cell death (Genini et al., 2000; Mansson et al., 2003).

2.3 Bromodeoxyuridine as a diagnostic tool

Bromodeoxyuridine or 5-bromo-2'-deoxyuridine (BrdU) is a halogenated NA of deoxynucleoside, thymidine. The structures of both BrdU and thymidine are relatively similar, except that 5-methyl group of thymidine is substituted by bromine atom in BrdU, as shown in Figure 2.4 (Perez-Zamorano & Valverde-Garduno, 2015). Despite having structural similarity with thymidine, BrdU is different in its biological effects in terms of its incorporation into the nascent DNA. During the cell cycle, in which the DNA replication takes place, BrdU competes with the cell's endogenous nucleoside

Table 2.1: Different nucleoside analogues and therapeutic interests for cancers.

Nucleoside analogues	Cancer treatment	Reference
5-Fluorouracil	Colorectal cancer	Bian et al. (2016)
Abacavir	Prostate cancer	Carlini et al. (2010)
Azidothymidine	Esophageal cancer	Wang et al. (2017)
Bromodeoxyuridine	Breast cancer	Zhou et al. (2018)
Capecitabine	Brest cancer	Galmarini et al. (2002)
Cisplatin	Cervical cancer	Zhu et al. (2016)
Cladribine	Acute myeloid cancer	Seligson et al. (2017)
Clofarabine	Breast cancer	Lubecka et al. (2018)
Cytarabine	Breast cancer	Laakmann, Witzel & Muller (2017)
Decitabine	Colorectal cancer	Hosokawa et al. (2019)
Fludarabine	Chronic lymphatic leukemia	Thompson et al. (2016)
Gemcitabine	Pancreatic cancer	Amrutkar & Gladhaug. (2017)
Lamivudine	Liver cancer	Zhang et al. (2019)
Troxacitabine	Pancreatic cancer	Adema et al. (2007)
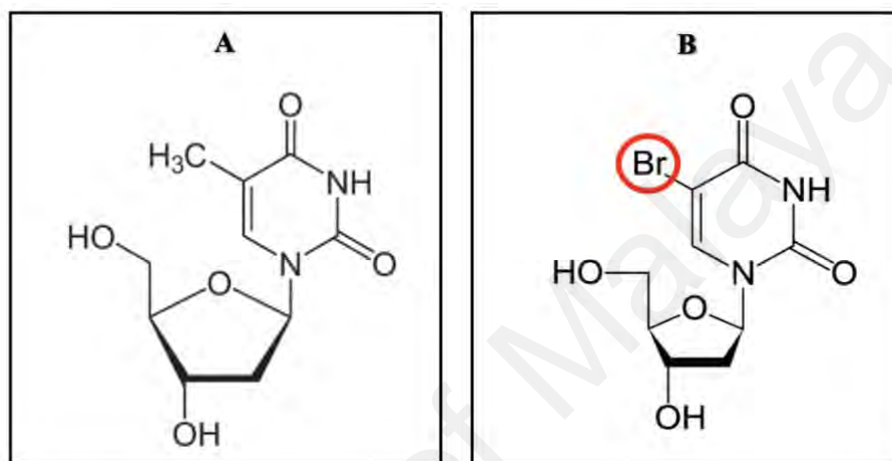
Figure 2.4: Chemical structures of (A) Thymidine and (B) Bromodeoxyuridine.

(thymidine) in selection and incorporation into newly forming DNA (Crane & Bhattacharya, 2013). The large size of halogen attached to BrdU influences the rate of DNA synthesis by disturbing methylation and transcriptional activity. This bromine atom efficiently absorbs more energy than hydrogen, which leads to increase its susceptibility towards radiation and DNA strand breakage as well as cell death (Yuan et al., 2016). BrdU readily crosses the blood brain barrier and its mechanism of action is led by TK1, in which the formation of BrdU triphosphate prolongs the G1-phase during the cell cycle, thus causes the impairment of the proliferative capacity and inhibition of DNA synthesis (Levkoff et al., 2008; Jagarlamudi & Shaw, 2018). Its incorporation into newly synthesized DNA strands, which mainly occurs during S-phase of the cell cycle, makes BrdU as a targeted drug in determining cancer cell proliferation that has been studied for over the past two decades (Cavanagh et al., 2011). As a tracker of cell division, through incorporation into DNA chain, followed by immunohistochemical detection with anti-BrdU antibodies, BrdU has been widely used in clinical fields as an anti-viral and chemotherapeutic agent (Haye-Bertolozzi & Aparicio, 2018). The use of BrdU in targeting cell proliferation in breast tumours has been reported in several published papers (Lloveras, Edgerton & Thor, 1991; Thor et al., 1999; Diermeir et al., 2003). BrdU can be administered either via intraperitoneal, intracerebroventricular or intravenous route by injection or orally (Taupin, 2007; Cavanagh et al., 2011).

2.4 Ligand transport in human blood circulation

Delivery of various endogenous and exogenous compounds such as drugs, hormones and fatty acids in human blood circulation is mainly assisted by plasma proteins. The efficacy of a drug in human blood circulation is influenced by its binding to the plasma proteins (Kragh-Hansen, Chuan & Otagiri, 2002; Mothi et al., 2005; Kallubai et al., 2018). Drug-protein interaction may have a major effect on its dissemination, transmission, as well as body removal (Nagati et al., 2018). It may also lead to the

alteration in the pharmacokinetics, pharmacodynamics, toxicity and stability of the drug in the human system (Hu et al., 2012). It is especially important for compounds which are poorly soluble in aqueous environments. On the other hand, duration of the therapeutic effect of a drug can be prolonged due to the protection of the protein-bound drug against rapid metabolism of the body's detoxification system (Lindup & Orme, 1981). Even though there are several transport proteins, present in the blood circulation *viz.*, human serum albumin, lipoproteins and α-1-acid glycoprotein, human serum albumin is the major protein carrier due to its high affinity and ligand binding competence as well as capacity to reversibly bind a large number of molecules with varying structural features (Kragh-Hansen, 1990; Korolenko et al., 2007).

2.5 Human serum albumin

Human serum albumin (HSA) is a monomeric, multi-domain transport protein, present in blood plasma. It plays an important role as the main determinant of the plasma osmotic pressure and modulates the distribution of fluid between body compartments as well as transporting and binding of both endogenous and exogenous compounds and cultivating the blood pH (Peters, 1996; Quinlan et al., 2005). It is produced in the liver and comprises of more than 50 % of the total plasma protein concentration (Quinlan et al., 2005; Yegonni et al., 2016). The molecular and structural properties of HSA are described below.

2.5.1 Physicochemical properties of HSA

The important physicochemical properties of HSA are outlined in Table 2.2. It is a monomeric protein with a molecular mass of 66, 479 Da, as retrieved from the matrix-assisted laser desorption / ionization-time of flight (MALDI-TOF) mass spectrometry (Dockal et al., 1999). The unique shape of HSA is arranged in a globular heart-shaped conformation with the approximate dimensions of 80 × 80 × 30 Å (He & Carter, 1992; Sugio et al., 1999). The axial ratio of HSA was predicted as 3.5:1, based on the

frequency dispersion of the dielectric constant (Ferrer et al., 2001), while the value of the radius of gyration is reported as 26.7 Å (Carter & Ho, 1994). Hydrodynamic parameters such as diffusion coefficient and sedimentation coefficient of HSA were described as 6.1×10^{-7} cm^2 s^{-1} and 4.2 S, respectively (Hunter & McDuffie, 1959; Dabkowska, Adamczyck & Kujda, 2013). The protein's globular structure was suggested based on the values of the frictional ratio and intrinsic viscosity, which were determined to be 1.37:1 (Hunter & McDuffie, 1959) and 0.056 dl g^{-1} (Hunter & McDuffie, 1959), respectively. Native form of HSA possesses an isoelectric point of 4.7 (Peters, 1996) and 5.8 for defatted HSA (Gianazza et al., 1984), while the isoionic point of 5.2 (Putnam, 1975). The secondary structures of HSA were divided into 67 % α-helices, 10 % β-sheets and 23 % flexible regions (Carter & Ho, 1994). The net charge of HSA at physiological pH (pH 7.4) and from its amino acid sequence was found to be −19 and −15, respectively, which suggested high solubility to the protein in aqueous environment (Tanford, 1950; Peters, 1996). The value of the partial specific volume of HSA was obtained as 0.733 cm^3 g^{-1} (Matthews, 1968). The specific extinction coefficient of HSA at 280 nm was found to be 5.3, which reflected the presence of Trp and Tyr residues (Wallevik, 1973).

Table 2.2: Physicochemical properties of HSA.

Property	Value	Reference
Molecular mass		
− Amino acid composition	66, 438 Da	Minghetti et al. (1986)
− MALDI-TOF	66, 479 Da	Dockal et al. (1999)
Overall dimension	$80 \times 80 \times 30$ Å	He & Carter (1992)
Axial ratio	3.5:1	Ferrer et al. (2001)
Radius of gyration	26.7 Å	Carter & Ho (1994)
Sedimentation coefficient, $S_{20,W}$	4.2 S	Hunter & McDuffie (1959)
Diffusion coefficient, $D_{20,W}$	6.1×10^{-7} cm^2 s^{-1}	Dabkowska et al. (2013)
Partial specific volume, $\bar{v}_2$	0.733 cm^3 g^{-1}	Matthews (1968)
Frictional ratio,	1.37:1	Hunter & McDuffie (1959)
Intrinsic viscosity, $[\eta]$	0.056 dl g^{-1}	Hunter & McDuffie (1959)
Isoelectric point		
− Native	4.7	Peters (1996)
− Defatted	5.8	Gianazza et al. (1984)
Isoionic point	5.2	Putnam (1975)
α-Helix	67 %	Carter & Ho (1994)
β-Sheet	10 %	Carter & Ho (1994)
Net charge per molecule		
− at pH 7.4	−19	Tanford (1950)
− Amino acid sequence	−15	Peters (1996)
$\varepsilon_{1\,cm}^{1\,\%}$ at 280 nm	5.3	Wallevik (1973)

2.5.2 Structural organization of HSA

The primary structure of HSA is comprised of a single polypeptide chain with a total of 585 amino acid residues (Figure 2.5). These residues form nine flexible loops and are arranged in a distinct pattern with eight sequential Cys-Cys pairs, linked together with 17 disulphide bridges. The three homologous domains of HSA are formed prior to their further grouping into nine loops and are indicated as domain I (1–195), domain II (196–383) and domain III (384–585). Each of these domains are further categorized into two separate subdomains, named as subdomain 'A' and subdomain 'B' (Carter & Ho, 1994). The first two long-short-long loops of subdomain 'A' such as loops 1–2, 4–5 and 7–8 are distributed as subdomains IA, IIA and IIIA, respectively, while the third loop (loops 3, 6 and 9) of subdomain 'B' are referred to as subdomains IB, IIB and IIIB, respectively (Dugaiczyk et al., 1982). The two subdomains are comprised of 6 and 4 α-helices (Figure 2.6), respectively, in which the composition of four helices in both subdomains (h1–h4) is identical, while the two other short helices in subdomain 'A' (h5 and h6) are arranged in non-identical fashion (Carter & Ho, 1994). The structure of HSA is stabilized by 17 intramolecular disulfide bonds, which are produced by 34 Cys out of 35 Cys residues (Quinlan et al., 2005). The crystallographic structure of HSA displays a heart-shaped pattern, formed from three homologous domains I, II, and III along with a pair of subdomains, 'A' and 'B', as shown in Figure 2.7 (Carter & Ho, 1994; Peters, 1996).
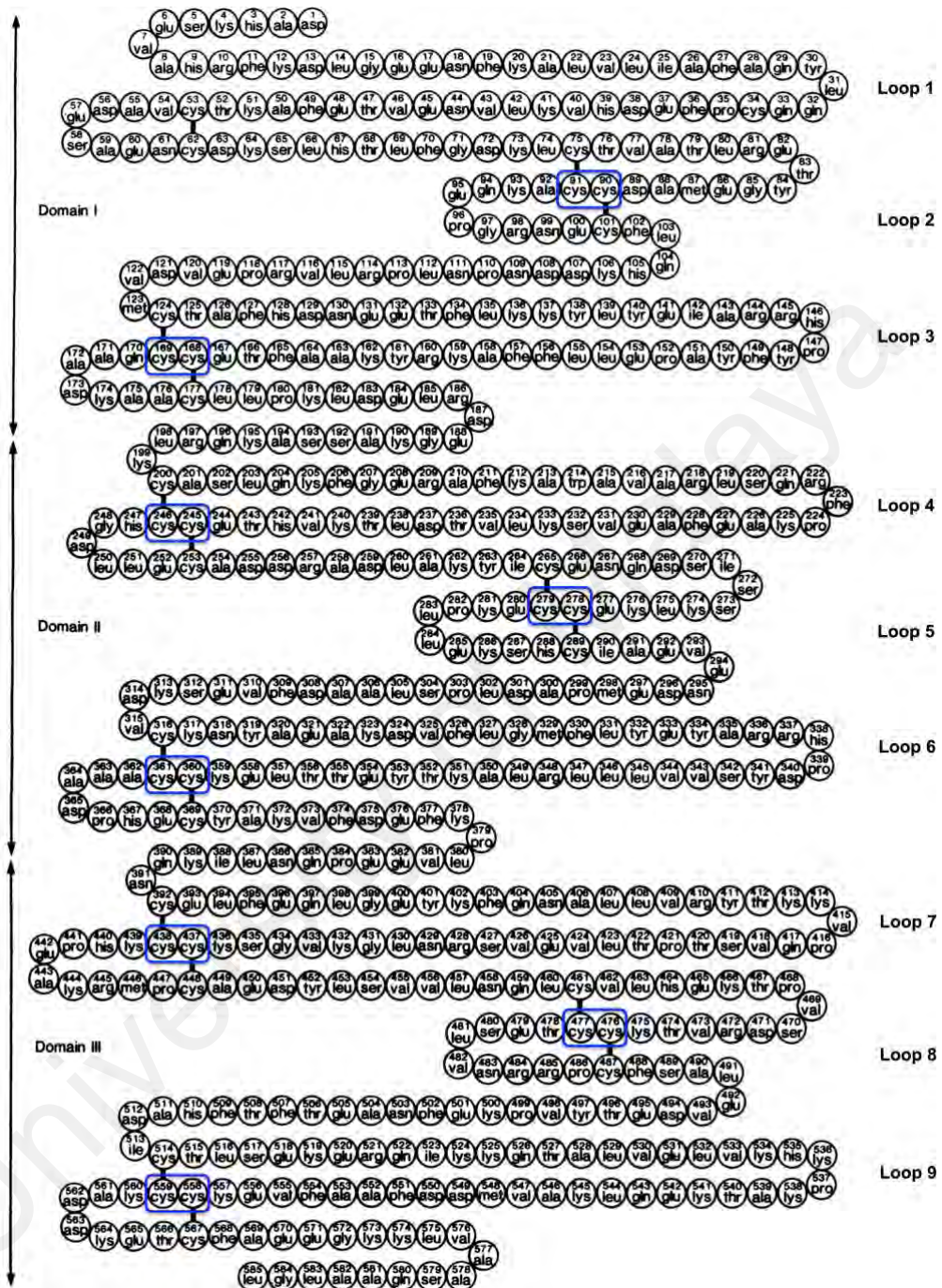
Figure 2.5: Amino acid sequence and disulphide bonding pattern of HSA. The blue-coloured box refers to the Cys-Cys pairs. (Adapted from Dugaiczyk et al., 1982).
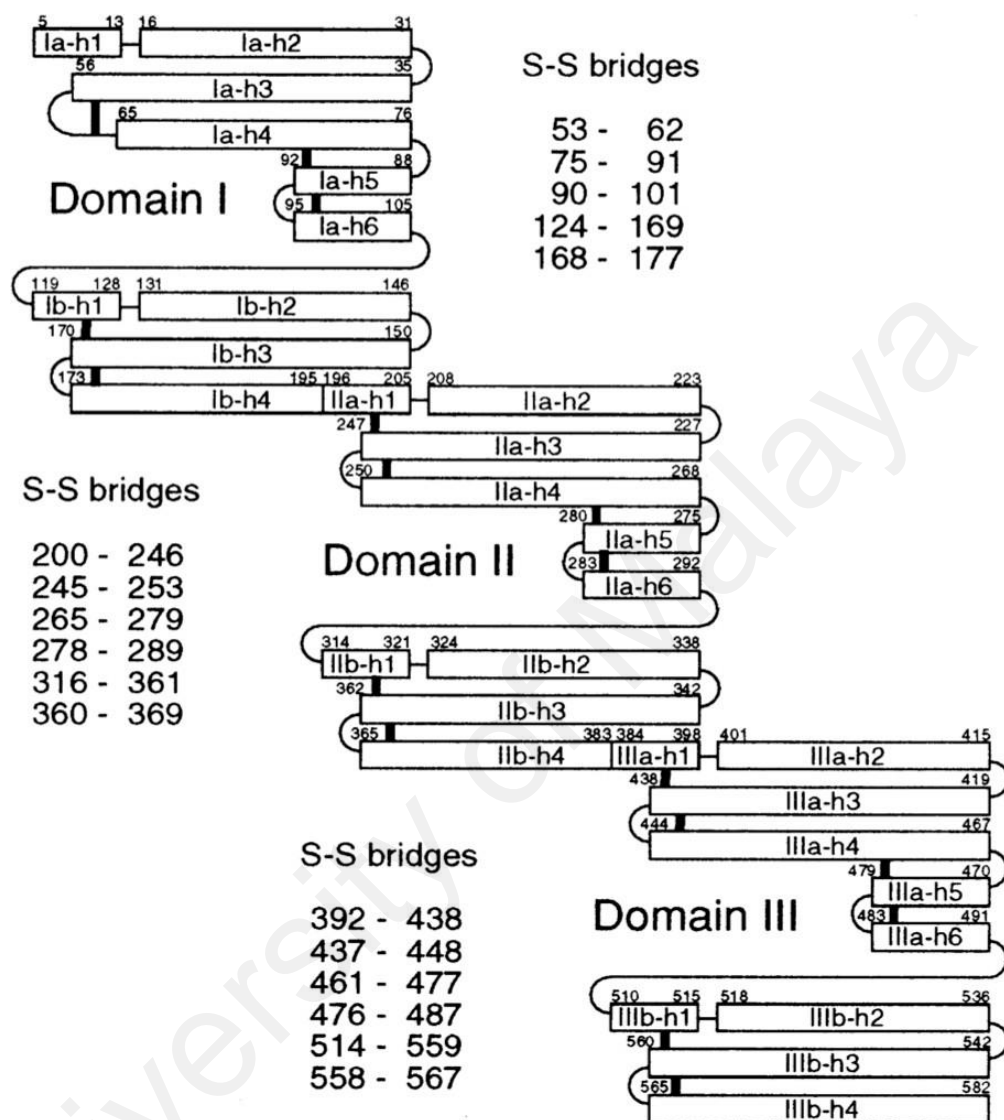
Figure 2.6: Diagram showing helices and disulphide bridges of HSA. Helices are illustrated by rectangles, and loops and turns by thin lines. Disulphide bridges are drawn with thick lines. (Adapted from Sugio et al., 1999).
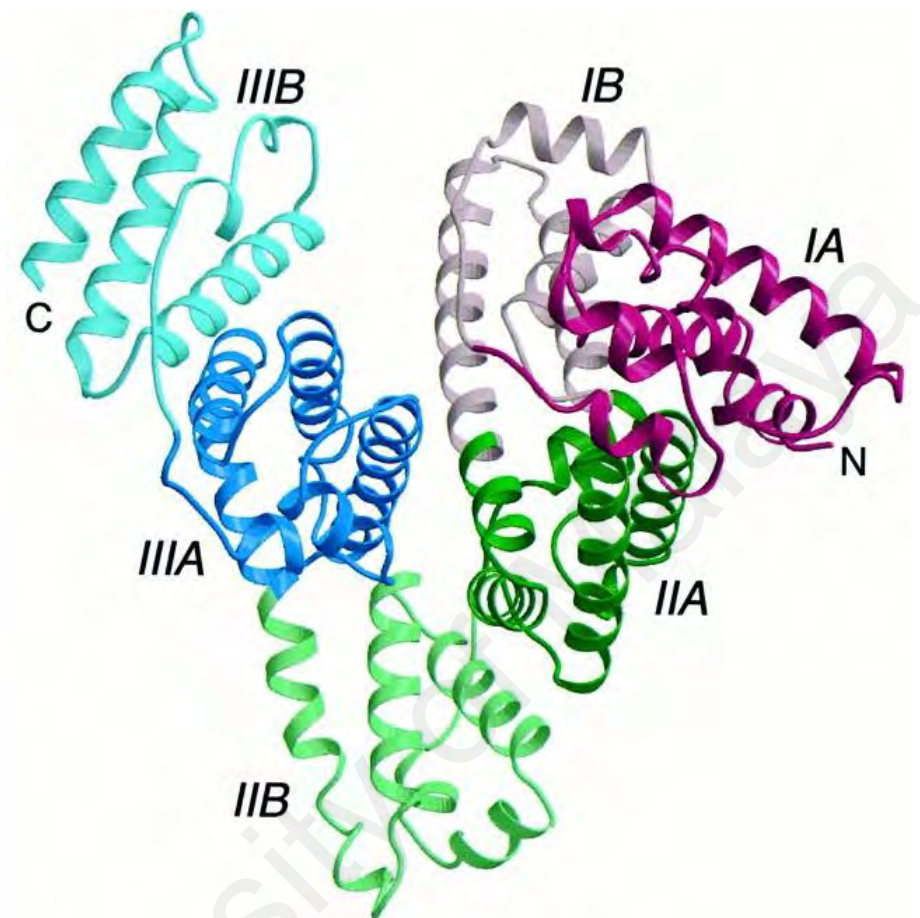
Figure 2.7: Three-dimensional structure of HSA. Each domain is marked with different colors; domain I (red), domain II (green), domain III (blue). Subdomains A and B of each domain are represented in 'dark' and 'light' shades. The N- and C-termini are marked as N and C, respectively. (Taken from Bhattacharya et al., 2000).

2.5.3 Functions of HSA

The protein, HSA plays an important role in providing physiological and pharmacological functions in the body. These functions include regulating the colloid osmotic pressure, maintaining the blood pH as well as transport and binding of both endogenous and exogenous compounds (Figge et al., 1991; Quinlan et al., 2005). It is also capable of providing protection against reactive oxygen species by acting as an antioxidant and in blood coagulation due to possessing the similar structure to heparin (Nicholson et al., 2000). Besides, it also acts as solubilizer by offering solubility to the ligands with poor aqueous solubility, such as fatty acids, amino acids and steroids. It transports metal ions such as zinc, calcium, iron and copper through the blood plasma (Peters, 1996) and functions as a depot protein to the key signalling molecule, nitric oxide (Stamler et al., 1992).

2.5.4 Ligand binding sites of HSA

There are two principal ligand binding sites in HSA, which are high adaptable to accommodate and bind different molecules, *i.e.*, Sudlow's sites I and II (Kragh-Hansen et al., 2002; Sudlow et al., 1975). Crystallographic studies have revealed that these binding sites reside in the hydrophobic cavities of the subdomains IIA (Sudlow's site I) and IIIA (Sudlow's site II), respectively, of HSA (Figure 2.8). It is suggested that the ligand-protein interactions are reversible in nature and the association constant ranges between 10^4 to 10^6 M^{-1} (Carter & Ho, 1994; Kragh-Hansen et al., 2002). Further details of the ligand binding sites I and II are described in the following subsections.

2.5.4.1 Site I

Site I is characterized as a high-affinity binding site, in which the entrance of the hydrophobic ligand binding pocket is surrounded by positively-charged residues. It consists of two nonpolar clusters along with a pair of centrally located polar residues. The inner cluster at the bottom of the pocket contains Tyr-150, His-242 and Arg-257 residues, while the outer cluster at the entrance of the pocket is comprised of Lys-195, Lys-199, Arg-218 and Arg-222 residues (Kragh- Hansen et al., 2002; Ghuman et al., 2005). Thus, this also favours the binding of negatively charged heterocyclic molecules. Site I has the ability to bind various ligands including large molecules due to being more flexible, wider and greater compared to other sites (Kragh-Hansen et al., 1988). It is also reported that site I has two overlapping binding sites of warfarin and azapropazone binding (warfarin-azapropazone binding area), with the presence of single Trp residue (Trp-214) in the non-overlapping region of the warfarin site (Fehske et al., 1982). On the other hand, Yamasaki et al. (1996) have suggested the presence of three binding regions, *viz.*, Ia, Ib and Ic for the binding of warfarin, azapropazone and butamben, respectively, in site I.
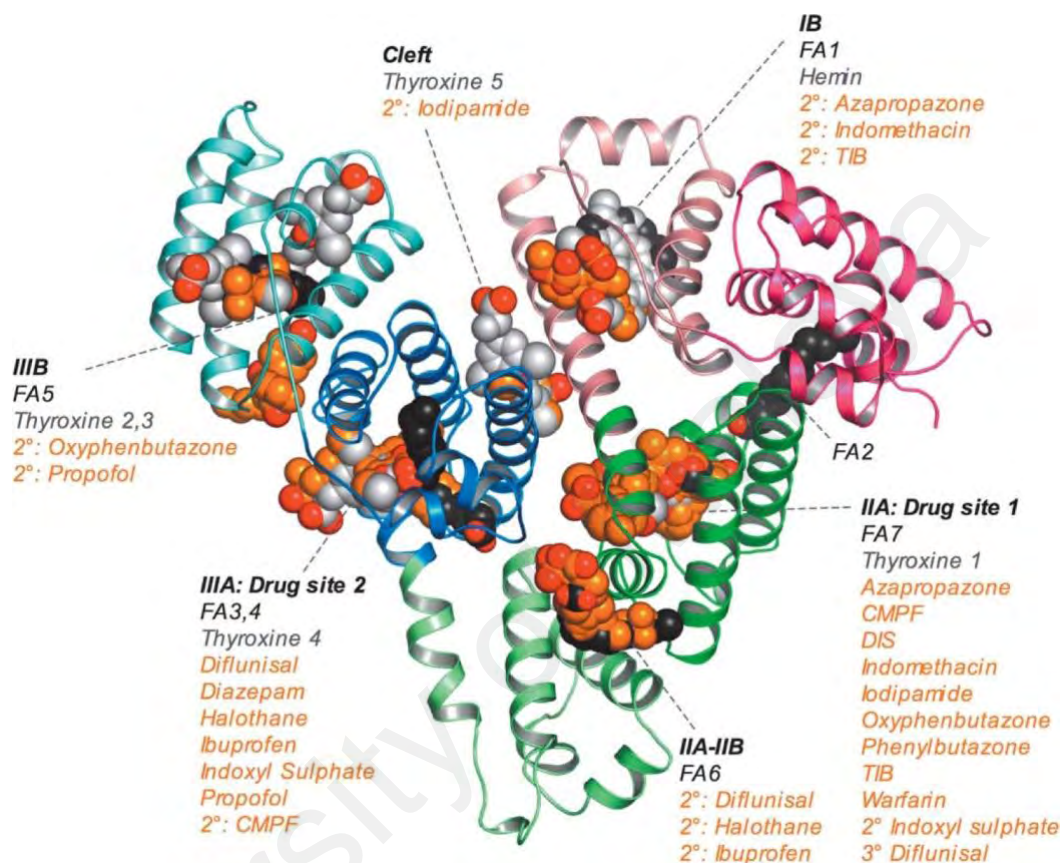
Figure 2.8: Diagram showing ligand binding sites of HSA. Individual subdomains are marked with different coloration and ligands are depicted as space-filling models. Oxygen atoms are displayed in red colour. All other atoms in fatty acids, other endogenous ligands (hemin and thyroxine) and drugs are shown in black, grey and orange colours, respectively. (Adapted from Ghuman et al., 2005).

2.5.4.2 Site II

Ligands such as diazepam, ibuprofen and ketoprofen preferably bind to site II, located in subdomain IIIA of HSA. The smaller size and lesser flexibility of this binding site cause large molecules to be less likely bound to its binding pocket (Kragh-Hansen et al., 2002). Site II is preferred by binding of aromatic carboxylic acids to a negatively charged group at one end of the molecule away from the hydrophobic centre (Kragh-Hansen et al., 2002). The hydrophobic binding pocket consists of a single dominant polar patch near the entrance that centered around Arg-410 and Tyr-411 residues (Sugio et al., 1999). The lack of binding of large molecules to this site is also due to the absence of any overlapping binding sites and its narrower size (Kragh-Hansen et al., 2002).

Besides, the flexibility of site II is lesser than site I and is usually influenced by stereoselectivity, as suggested by the stronger binding affinity of L-Trp (~100 times higher) compared to its D-isomer (Kragh-Hansen et al., 2002). In addition, a slight modification of the ligands or substitution with a small group may greatly affect their binding to site II. This can be exemplified from the report that the binding of fluorinated diazepam remained unsuccessful, albeit the preferred binding site of diazepam is site II (Chuang & Otagiri, 2001).

2.5.5 Pharmacological importance of ligand-HSA interaction

HSA is known to be an ideal transporter for a variety of ligands in blood circulation due to its binding selectivity to neutral and acidic lipophilic compounds (Kragh-Hansen et al., 2002; Olson & Christ, 1996). Interaction of a drug to protein helps in enhancing its pharmacokinetic properties such as the *in vivo* half-life of a therapeutic drug is increased upon binding to HSA. The binding can prolong the duration and efficacy of the drug. Besides, the binding between drug and protein is also beneficial in terms of solubility, toxicity reduction and elimination of the drug from the human body (Kragh-

Hansen et al., 2002; Olson & Christ, 1996; Peters, 1996). If the concentration of the administered drug *in vivo* is lower than in HSA, the binding shows higher affinity binding (Kragh-Hansen et al., 2002). Therefore, the study of ligand-protein interaction has become an interesting subject in order to understand the physiological action of pharmaceutical compounds at the molecular level in the human body.

Albeit several reports have been made on the investigation of BrdU effectiveness and functions in human cells, its interaction with HSA is yet to be explored. In view of it, this study aims to understand the binding characteristics of the interaction between BrdU and HSA. Hence, the binding affinity and binding forces between BrdU and HSA and its binding site are well characterized. Furthermore, the changes in HSA's microenvironmental structures upon BrdU binding as well as the influence of metal ions on BrdU−HSA binding affinity are also revealed.

CHAPTER 3: MATERIALS AND METHODS

3.1 Materials

3.1.1 Protein, drugs and other reagents

Fatty acid and globulin free albumin from human serum (HSA) (purity $\geq$ 99 %; Lot # 068K7538V), warfarin (WFN) (purity $\geq$ 99 %; Lot # 104K1261) and indomethacin (IDN) (purity $\geq$ 99 %; Lot # 115K0689) were purchased from Sigma-Aldrich Co. (St Louis, USA). Diazepam (DZM) (purity $\geq$ 98 %; Lot # 1071B02) was the product of Lipomed AG (Arlesheim, CH). Bromodeoxyuridine (BrdU) (purity $\geq$ 99 %; Batch # S791804) was procured from Selleckchem (Houston, USA).

Various metal chloride salts such as barium chloride ($BaCl_2$), calcium chloride ($CaCl_2$), copper (II) chloride ($CuCl_2$), magnesium chloride ($MgCl_2$), manganese (II) chloride ($MnCl_2$) and potassium chloride (KCl) were obtained from Sigma-Aldrich Co. (St. Louis, USA). Sodium dihydrogen phosphate and *di*-sodium hydrogen phosphate were purchased from SYSTERM® (Shah Alam, MY). Standard buffers of pH 7.0 and pH 10.0 were supplied by Reagecon (Shannon, IE). Dimethyl sulphoxide (DMSO) was procured from Merck Millipore (Darmstadt, DEU).

3.1.2 Miscellaneous

Polyvinylidene fluoride (PVDF) membrane filters (0.45 μm pore size) were purchased from Merck Millipore (Darmstadt, DEU), whereas cellulose nitrate membrane filters (0.45 μm pore size) were supplied by Whatman® (Buckinghamshire, UK). Parafilm "M" Laboratory Film was obtained from Bemis Company Inc. (Neenah, USA).

Ultrapure (Type 1) water produced by Milli-Q Water Purification System (Merck Millipore, Darmstadt, DEU) was used throughout this study.

All experiments were performed in 0.06 M sodium phosphate buffer, pH 7.4 (PB 7.4) at 298 K, unless otherwise stated.

3.2　Methods

3.2.1 pH measurements

The pH of the buffer solution was measured on a Sartorius Basic Meter PB-10, connected to a Sartorius pH / ATC electrode (Sartorius AG, Germany). Standard buffers of pH 7.0 and pH 10.0 were used to calibrate the pH meter for pH measurements in the neutral and alkaline pH ranges, respectively. The least count of the pH meter was 0.01 pH unit.

3.2.2　Preparation of protein stock solution

A known amount of HSA crystals were dissolved in a fixed volume of PB 7.4 in standard flask to prepare the stock solution. The solution was filtered through PVDF membrane filter and its concentration was determined spectrophotometrically on Shimadzu spectrophotometer (model UV-2450), using a molar extinction coefficient, ϵ_m of 36, 500 M^{-1} cm^{-1} at 280 nm (Painter et al., 1998).

3.2.3 Preparation of ligand solutions

The stock solutions (5 mg / 5 ml) of BrdU and other pharmaceuticals (WFN, IDN and DZM) were prepared in DMSO and were diluted with PB 7.4 to get the working solutions of the desired concentration. The final concentration of DMSO was < 1 % in experiments involving these ligands.

3.2.4 Fluorescence spectral measurements

The fluorescence spectra were generally recorded at 298 K on a Jasco spectrofluorometer (model FP-6500), equipped with a 10 mm path length quartz cuvette. The excitation wavelength used was 295 nm for the protein (HSA) fluorescence measurements in the wavelength range of 310–400 nm and 335 nm for the WFN fluorescence measurements in the wavelength range of 360–480 nm. Other parameters were set in the following way: excitation and emission bandwidths = 10 nm each; data pitch = 1 nm; scan speed = 500 nm min^{-1} and detector voltage = 240 V. A circulating

water bath (Protech 632D) was attached to the instrument for maintaining the sample temperature.

The wavelength ranges used for excitation and emission in three-dimensional (3-D) fluorescence spectral measurements were 220 – 350 nm with a data pitch of 5 nm and 220−500 nm with a data pitch of 1 nm, respectively. The concentrations of protein and BrdU were 3 μM and 9 μM, respectively, in these experiments.

3.2.5 Absorption spectral measurements

The ultraviolet-visible (UV-Vis) absorption spectra of either HSA / BrdU (15 μM) or BrdU−HSA (1:1) mixture were recorded on Shimadzu spectrophotometer (model UV-2450), using a pair of 10 mm path length quartz cuvettes in the wavelength range of 240–315 nm in PB 7.4 at 298 K. Alternatively, the UV-Vis absorption spectra of HSA (15 μM), BrdU (15–75 μM with 15 μM interval) and BrdU−HSA (1:1, 2:1, 3:1, 4:1 and 5:1) mixtures were also recorded in the same wavelength range in PB 7.4 at 298 K.

The UV-Vis absorption spectra of protein solution (3 μM) and BrdU−HSA mixtures with increasing concentrations of BrdU (3–33 μM with 3 μM interval) were also recorded in the wavelength range of 295–400 nm. These spectra were used for inner filter correction in the fluorescence spectra, as described in Section 3.2.7.2.

3.2.6 Circular dichroism spectral measurements

The circular dichroism (CD) measurements were executed with a Jasco spectropolarimeter (model J-815), equipped with a thermostatically-controlled cell holder. Cuvettes with a path length of 1 mm and 10 mm were employed for CD measurements in the far-UV (200−250 nm) and the near-UV (250−300 nm) regions, respectively. The protein concentration used was 1 μM and 8 μM for far-UV and near-UV CD measurements, respectively. Both CD spectra were recorded for the protein solution using the same concentrations as well as BrdU−HSA (1:1 and 3:1) mixtures.

Each spectrum, representing the average of four scans was collected with a scan speed of 100 nm min^{-1} and a time response of 0.5 s at 298 K.

3.2.7 BrdU−HSA interaction studies

The interaction between BrdU and HSA was studied using fluorescence quenching titration method (Feroz et al., 2015), as described below.

3.2.7.1 Fluorescence quenching titration

The fluorescence quenching titration was performed by taking a fixed volume (300 μl) of the stock HSA solution (30 μM) in different tubes. Increasing volumes (90–990 μl with 90 μl interval) of the stock BrdU solution (100 μM) were added to these tubes in order to get the final concentration of BrdU as 3−33 μM with 3 μM interval. The total volume in each tube was made to 3 ml with buffer (PB 7.4) and vortexed for homogeneous mixing. The fluorescence spectra were collected at three different temperatures in the wavelength range, 310−400 nm after 30 min incubation of the solution mixtures at respective temperatures *i.e.* 288, 298 and 308 K.

3.2.7.2 Data analysis

I. *Inner filter effect correction*

The fluorescence spectra were subjected to inner filter effect correction according to the method suggested by Lakowicz (2006). The values of the observed fluorescence intensity (F_{obs}) and the absorbance values at the excitation (A_{ex}) and the emission (A_{em}) wavelengths were substituted in the following equation, to get the values of the corrected fluorescence intensity (F_{cor}).

$$F_{cor} = F_{obs}\ 10^{(A_{ex}+A_{em})/2} \tag{1}$$

II. *Quenching and binding parameters*

The corrected fluorescence data were treated according to the Stern-Volmer equation. Values of the Stern-Volmer quenching constant (K_{sv}) were obtained from the

slope of the linear Stern-Volmer plots, obeying the following equation (Lakowicz, 2006):

$$F_0 / F = K_{sv} [Q] + 1 = k_q \tau_0 [Q] + 1 \qquad (2)$$

where F_0 and F are the fluorescence intensity values in the absence and the presence of the quencher (BrdU), respectively and $[Q]$ is the concentration of the quencher.

Dividing the K_{sv} value with the fluorescence life time (τ_0) of HSA (6.38×10^{-9} s) (Abou-Zeid & Al-Shihi, 2008) yielded the values of the bimolecular quenching rate constant, k_q.

The magnitude of the binding constant, K_a for the BrdU−HSA system at different temperatures was determined from the following double logarithmic equation (Bi et al., 2004):

$$\log (F_0 − F) / F = n \log K_a − n \log [1 ([L_T] − (F_0 − F) [P_T]/F_0) \qquad (3)$$

where n is the Hill coefficient, while $[L_T]$ and $[P_T]$ represent the total ligand and total protein concentrations, respectively.

III. _Thermodynamic parameters_

Values of thermodynamic parameters, _i.e._ enthalpy change (ΔH) and entropy change (ΔS) were obtained from the van't Hoff plot between ln K_a and 1 / T (Kabir et al., 2017). The free energy change (ΔG) of the binding reaction was calculated with the help of the following equation:

$$\Delta G = \Delta H − T \Delta S \qquad (4)$$

3.2.8 Thermal stability studies

Thermal denaturation of the protein (3 μM) and BrdU−HSA (3:1) mixture was studied in PB 7.4 by recording the fluorescence intensity at 343 nm at different temperatures between 298 and 353 K in steps of 1 K. An equilibration time of 3 min was fixed at each temperature before spectral measurements.

The fluorescence intensity values were transformed into relative fluorescence intensity (Relative FI) by taking the fluorescence intensity of HSA / BrdU−HSA mixture at 298 K as 100 and were plotted against temperature.

3.2.9 Ligand displacement studies

For ligand displacement experiments, equimolar (1:1) mixtures of marker ligands (WFN / IDN / DZM) and HSA were used and titrated with increasing BrdU concentrations, as described in Section 3.2.7.1. A prior incubation of marker ligand−HSA mixture for 30 min was made at 298 K before each titration. The solution mixtures were further incubated for another 30 min after BrdU addition before recording the fluorescence spectra / fluorescence measurements.

Values of the fluorescence intensity at emission maxima, obtained at different BrdU concentrations were transformed into relative fluorescence intensity (Relative FI) by taking the fluorescence intensity in the absence of BrdU as 100. These values were plotted against BrdU concentration.

3.2.10 Computational studies

Docking, visualization and rendering simulation of BrdU to HSA were conducted using AutoDock4 (Morris et al., 2009). The 3-D crystal structure of HSA was retrieved from the Protein Data Bank (PDB ID: 1BM0, 2.5 Å). Avogadro (Hanwell et al., 2012) was utilized to retrieve the structure of BrdU following the geometrical structure optimization using MMFF94 force field (Halgren, 1996). Independent docking analysis was performed for each binding site (Sudlow's sites I and II). Assessment of the docking simulations was clustered based on the root-mean-squared deviation (RMSD) tolerance of 2.0 Å and the generated interactions were visualized using UCSF Chimera (Pettersen et al., 2004).

3.2.11 Metal ions interference studies

The influence of metal ions, such as Ba^{2+}, Mg^{2+}, K^+, Ca^{2+}, Mn^{2+} and Cu^{2+} on BrdU binding to HSA was studied using fluorescence quenching titration. The protein solution was mixed with the metal salt solutions in separate experiments and the mixtures were incubated for 1 h at 298 K. Titration with increasing BrdU concentrations was performed after a further incubation of 30 min before fluorescence spectral measurements, as described in Section 3.2.7.1. The final concentrations of the protein and the metal salts in the incubation mixtures were maintained as 3 µM and 30 µM, respectively. The selected [metal salt]:[HSA] molar ratio was chosen to obtain significant difference in the quenching patterns in the presence of different metal salts. Values of the binding constant, K_a for BrdU−HSA interactions in the absence and the presence of metal ions were obtained by treating the fluorescence quenching data according to equation (3), as described in Section 3.2.7.2.

3.2.12 Statistical analysis

The results for BrdU−HSA binding are expressed as a mean ± standard deviation (SD) from three independent experiments using the following formula:

$$\sigma = \sqrt{\frac{1}{N}\sum_{i=1}^{N}(x_i - \mu)^2}$$

Where x_i is an individual value, μ is the mean value and N is the total number of values. Statistical data processing, curve fitting and smoothing were analyzed using OriginPro version 8.5 software (OriginLab Corporation, Northampton, USA).

CHAPTER 4: RESULTS AND DISCUSSION

4.1 BrdU−HSA interaction

4.1.1 BrdU-induced quenching of HSA fluorescence

Quenching of the protein fluorescence upon addition of a ligand may occur due to excited-state reaction, molecular rearrangement, energy transfer and ground-state complex formation (Lakowicz, 2006). Intrinsic fluorescence of a protein is mainly contributed by tyrosine (Tyr) and tryptophan (Trp) residues. However, it is solely due to Trp residues, when the protein is excited at 295 nm (Lakowicz, 2006). Since HSA contains a single Trp residue (Trp-214), located in the hydrophobic cavity in subdomain IIA (Bell & Brenner, 1982), protein's fluorescence characteristics were exploited after titrating it with increasing concentrations of BrdU.

Occurrence of the emission maxima at 343 nm in the fluorescence spectrum of HSA (Figure 4.1) was reflective of the presence of Trp in the protein. Continuous decline in the fluorescence intensity characterized the fluorescence spectra of the protein upon addition of increasing BrdU concentrations (Figure 4.1). About ~52% quenching in the protein fluorescence along with 3 nm blue shift were observed at 33 μM BrdU concentration at 298 K (Figure 4.1). Both these changes in the fluorescence characteristics of HSA were reflections of ligand binding to the protein. Microenvironmental alteration around Trp-214 residue of the protein may account for such changes in the protein fluorescence (Khanna, Tokuda, & Waisman, 1986).

4.1.2 Quenching mechanism

Ligand-induced quenching of the protein fluorescence can be characterized as either static or dynamic, which can be differentiated on the basis of their temperature dependence (Lakowicz, 2006). Higher temperature leads to faster diffusion of molecules, thus increases the quenching constant in dynamic quenching. On the other hand, dissociation of ligand-protein complex is anticipated at higher temperature, which
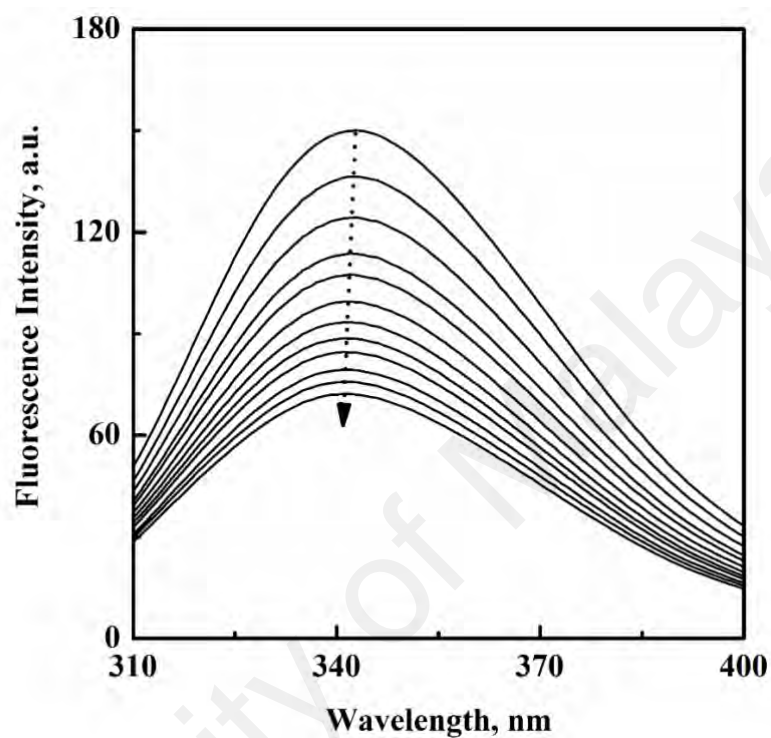
Figure 4.1: Fluorescence spectra of HSA (3 μM) in the absence and presence of increasing BrdU concentrations, upon excitation at 295 nm in PB 7.4 at 298 K. The BrdU concentrations from top to bottom were 0−33 μM with 3 μM interval.

leads to decrease in the quenching constant with temperature in static quenching.

To characterize the BrdU-induced quenching of HSA fluorescence, titration experiments were performed at two other temperatures, *i.e.* 288 and 308 K and the results are shown in Figures 4.2 and 4.3, respectively. Qualitatively similar changes in the fluorescence characteristics of HSA (fluorescence quenching and shift in the emission maxima) were noticed at these temperatures. Although the blue shift in the emission maxima was smaller (2 nm) at these temperatures, quantitative differences were found in the fluorescence quenching. Figure 4.4 shows changes in the relative fluorescence intensity at 343 nm (Relative $FI_{343\ nm}$) of HSA with increasing BrdU concentrations at three different temperatures. As can be clearly seen from the figure, maximum decrease in the Relative $FI_{343\ nm}$ was found at 288 K at all BrdU concentrations. This decrease became smaller with increase in temperature, as decrease in the Relative $FI_{343\ nm}$ value was lowest at 308 K at all BrdU concentrations (Figure 4.4).

Fluorescence quenching titration data were transformed according to the Stern-Volmer equation (2), as described in Section 3.2.7.2 and the resulting Stern-Volmer plots at three different temperatures are shown in Figure 4.5. All these plots showed linearity with a correlation coefficient ≥ 0.998 within the range of BrdU concentration, used in these experiments. This indicated involvement of one type of quenching mechanism in BrdU−HSA system. Table 4.1 shows the K_{sv} values, obtained from the slope of the Stern-Volmer plots (Figure 4.5) at three different temperatures. As reflected from Table 4.1 and inset of Figure 4.5, K_{sv} value progressively declined with increasing temperature, which was suggestive of the involvement of static quenching mechanism in BrdU−HSA system and thus BrdU−HSA complex formation. This result was in line with several published reports, suggesting involvement of static quenching mechanism in ligand-protein systems (Gan et al., 2019; Manjushree & Revanasiddappa, 2019;
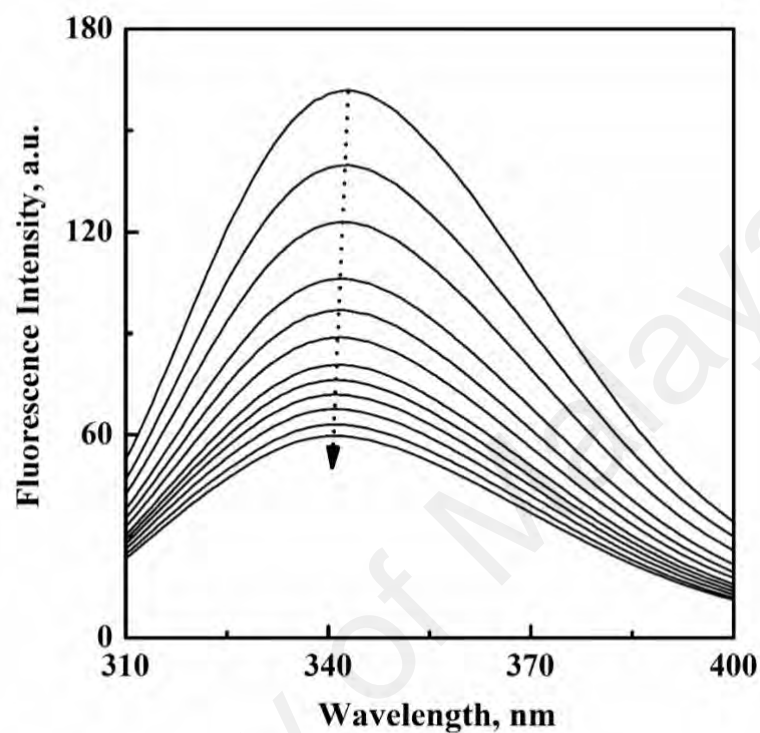
Figure 4.2: Fluorescence spectra of HSA (3 μM) in the absence and presence of increasing BrdU concentrations, upon excitation at 295 nm in PB 7.4 at 288 K. The BrdU concentrations from top to bottom were 0–33 μM with 3 μM interval.
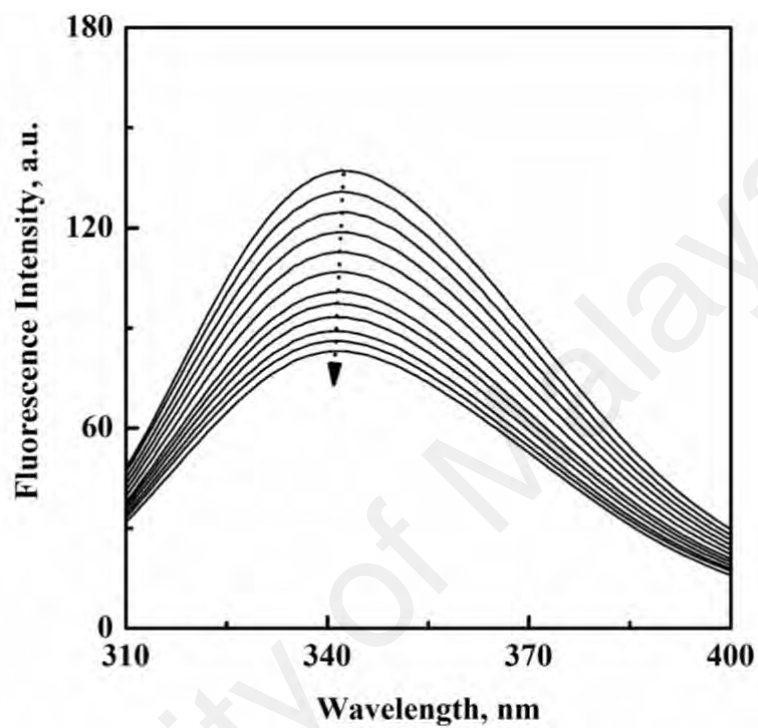
Figure 4.3: Fluorescence spectra of HSA (3 μM) in the absence and presence of increasing BrdU concentrations, upon excitation at 295 nm in PB 7.4 at 308 K. The BrdU concentrations from top to bottom were 0−33 μM with 3 μM interval.
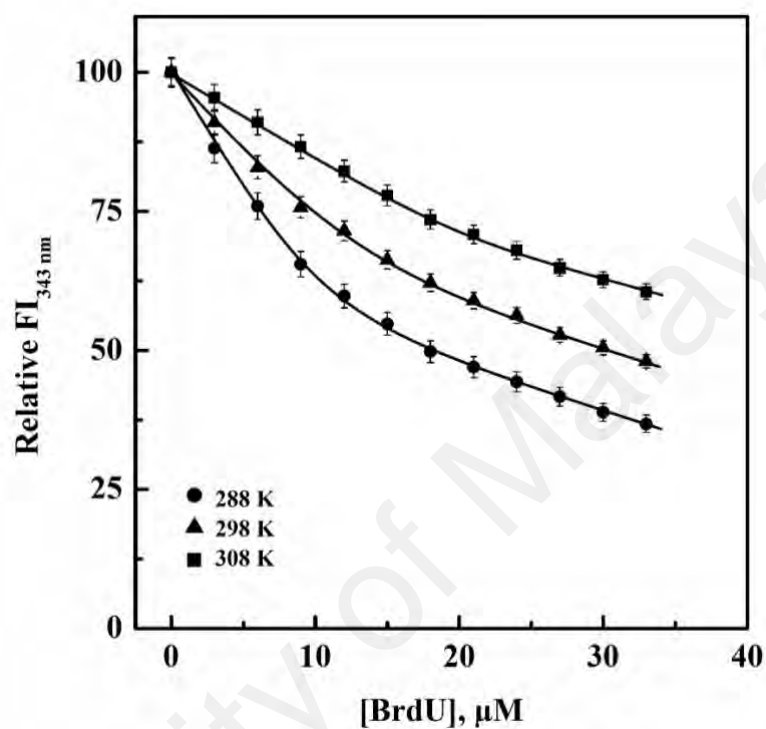
Figure 4.4: The diagram showing decrease in the relative FI$_{343\ nm}$ with increasing BrdU concentrations at three different temperatures. Values of the relative FI$_{343\ nm}$ at different BrdU concentrations were obtained from Figures 4.1−4.3.
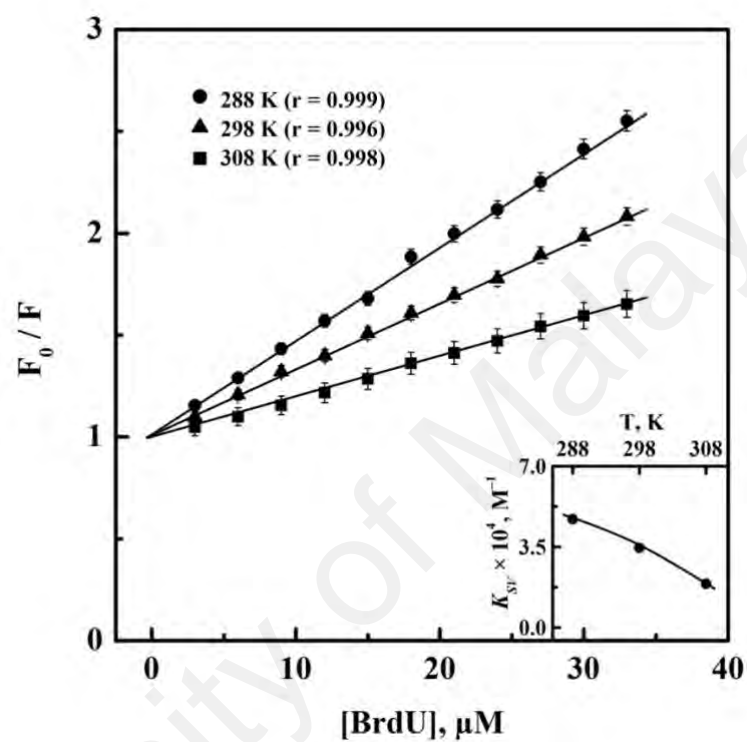
Figure 4.5: Stern-Volmer plots for BrdU–HSA system at three different temperatures, *i.e.* **288, 298 and 308 K. Inset shows the decrease in the** K_{SV} **value with increasing temperature.**

Table 4.1: Binding characteristics of BrdU−HSA system at three different temperatures, as studied in PB 7.4.

T (K)	$K_{sv} \times 10^4$ (M^{-1})	$k_q \times 10^{12}$ (M^{-1} s^{-1})	n	$K_a \times 10^4$ (M^{-1})
288	4.70 ± 0.12	7.37 ± 0.15	1.01 ± 0.03	3.97 ± 0.42
298	3.19 ± 0.06	5.00 ± 0.07	1.04 ± 0.05	3.18 ± 0.17
308	1.90 ± 0.20	2.98 ± 0.27	1.10 ± 0.06	2.49 ± 0.36

Agrawal et al., 2019). Values of the bimolecular quenching rate constant (k_q) for BrdU−HSA system were calculated following the method described in Section 3.2.7.2 and are given in Table 4.1. The k_q values had fallen in the order of 10^{12} at these temperatures, which were larger than the maximum dynamic quenching rate constant (2.0×10^{10} M^{-1} s^{-1}) (Zheng et al., 2014). These results further characterized BrdU-induced quenching of HSA fluorescence as static quenching. Additional support for the complex formation between BrdU and HSA was obtained from the UV-Vis absorption spectral results, as described below in Section 4.1.3.

4.1.3   UV-Vis absorption spectral analysis

To advocate the BrdU-induced quenching of HSA fluorescence as static quenching, changes in the UV-Vis absorption spectrum of HSA were monitored upon BrdU addition. Since the static quenching affects the ground state of the fluorophores, alterations in the protein absorption spectrum are inevitable upon complex formation (Lakowicz, 2006). Figure 4.6 depicts the UV-Vis absorption spectra of 15 μM HSA (blue line), 15 μM BrdU (green line) and BrdU−HSA (1:1) mixture (red line). To explore the above fact, the absorption spectrum of HSA was subtracted from the absorption spectrum of BrdU−HSA (1:1) mixture and the resultant difference absorption spectrum was compared with the absorption spectrum of free BrdU (Figure 4.6 inset). As can be seen from the inset of Figure 4.6, difference absorption spectrum showed a significant difference from the absorption spectrum of free BrdU, which suggested complexation of BrdU with the protein.

Further scrutiny about the effect of static quenching on the absorption spectrum of the protein was made by studying the absorption spectra of HSA in the absence and presence of increasing BrdU concentrations. Figure 4.7 (A) depicts the UV-Vis absorption spectra of HSA in the absence (blue line) and presence of increasing (15−75 μM) BrdU concentrations (red lines), while absorption spectra of free BrdU
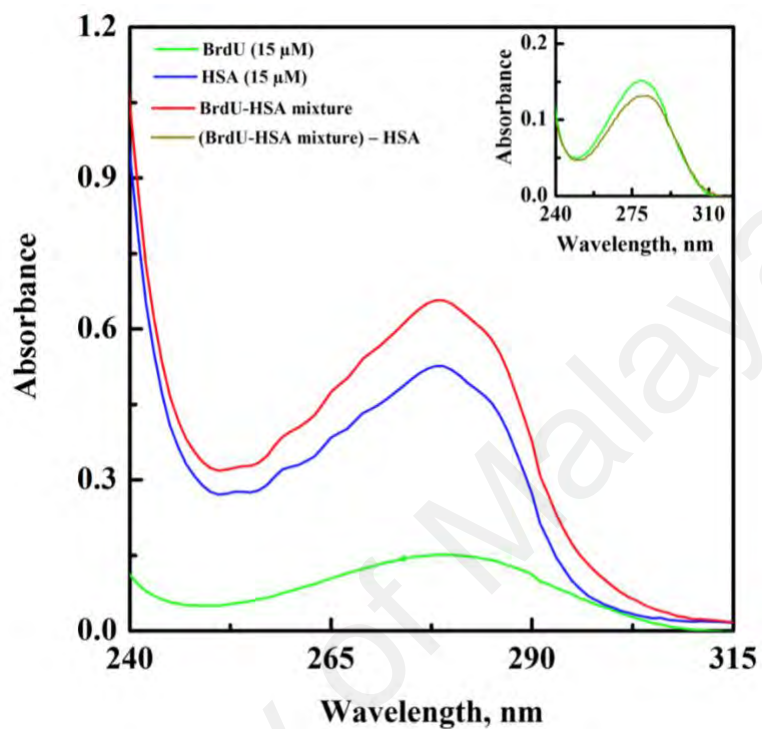
Figure 4.6: UV-Vis absorption spectra of BrdU–HSA (1:1) mixture (red line), 15 μM HSA (blue line) and 15 μM BrdU (green line), as studied in PB 7.4 at 298 K. Inset shows the comparison between the absorption spectrum of 15 μM BrdU and the difference spectrum, obtained after subtracting the absorption spectrum of 15 μM HSA from the absorption spectrum of BrdU–HSA (1:1) mixture.
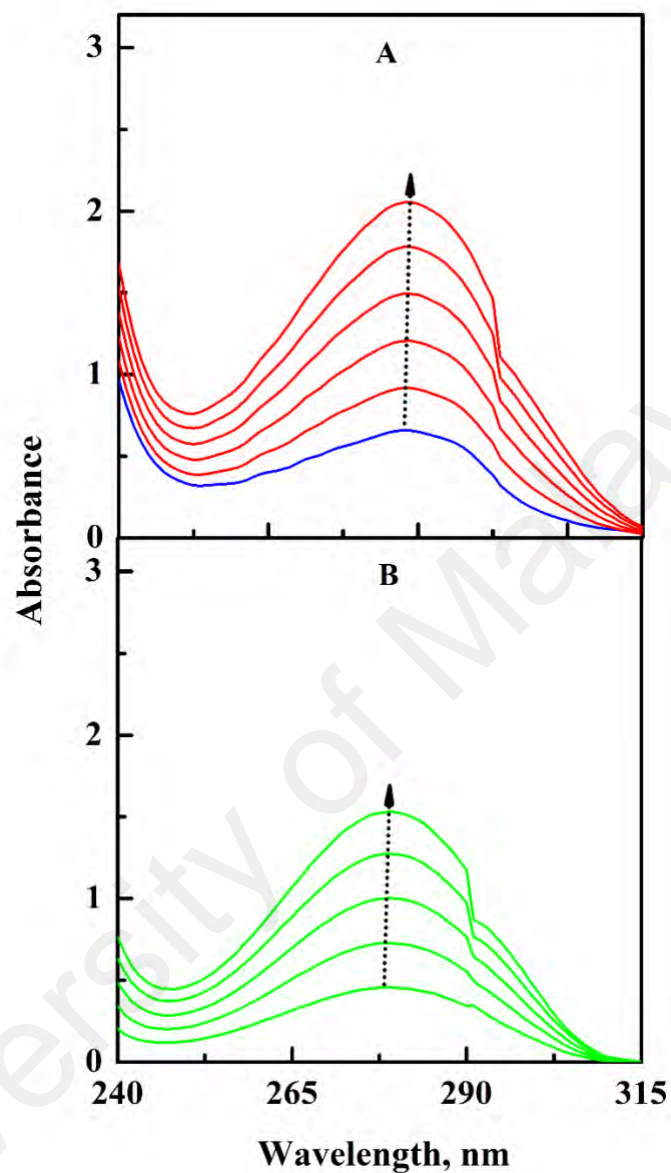
Figure 4.7: (A) UV-Vis absorption spectra of HSA (15 µM) in the absence (blue line) and the presence (red lines) of increasing concentrations (15−75 µM with 15 µM interval) of BrdU (from bottom to top). (B) UV-Vis absorption spectra (from bottom to top) of increasing BrdU concentrations (15−75 µM with 15 µM interval).

(15–75 μM) are displayed in Figure 4.7 (B). In order to see the effect of BrdU addition in the UV-Vis absorption spectra of HSA, absorption spectra of free BrdU (Figure 4.7 (B)) were subtracted from the UV-Vis absorption spectra of BrdU–HSA mixtures (Figure 4.7 (A)). The resulting spectra are shown in Figure 4.8. As evident from the figure, the absorption spectrum of HSA (blue line) showed hyperchromism after the addition of BrdU (red lines from bottom to top), thus supported the ligand-protein complex formation. Both these results suggested the involvement of static quenching mechanism and thus the formation of BrdU–HSA complex.

4.1.4 *Binding affinity and interaction forces*

If there are same and independent ligand binding sites (n) in the protein, the binding constant (K_a) of the ligand-protein system can be determined using double logarithmic equation (Bi et al., 2004). The double logarithmic plots, obtained after analyzing the fluorescence quenching data according to equation (3) are given in Figure 4.9 and the values of K_a and n at different temperatures are displayed in Table 4.1. Value of n was found to be close to 1.0 at all temperatures (Table 4.1), suggesting presence of a single binding site of BrdU on HSA. The K_a values were found in the range of 2.49 ± 0.36 − 3.97 ± 0.42 × 10^4 M^{-1} at these temperatures. The K_a values with the order of 10^4 M^{-1} demonstrated moderate binding affinity between HSA and BrdU (Zheng et al., 2014), which is useful to transfer the ligand from the transport protein to its receptor on the target organ / tissue. Many drug-binding studies have shown moderate binding affinity between the drug and transport protein (Zsila et al., 2009; Fu et al., 2014; Kabir et al., 2016). The gradual decrease of K_a value with increasing temperature in the BrdU−HSA system indicated destabilization of the ligand-protein complex at higher temperatures.

Information about the molecular forces involved in ligand-protein complex formation can be obtained from the thermodynamic data of the binding reaction (Ross
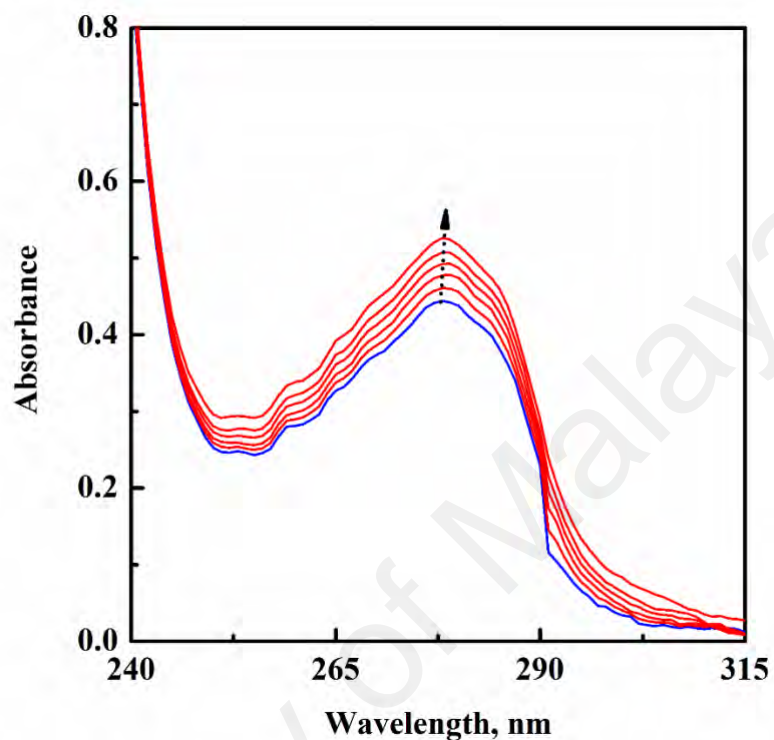
Figure 4.8: Effect of increasing concentrations (15−75 μM with 15 μM interval) of BrdU (red lines) on the UV-Vis absorption spectrum of HSA (15 μM) (blue line), as studied in PB 7.4 at 298 K. The spectra in the presence of BrdU were obtained after subtracting the UV-Vis absorption spectra of free BrdU (Figure 4.7 (B)) from the UV-Vis absorption spectra of BrdU−HSA mixture (Figure 4.7 (A)), containing similar concentrations of BrdU.
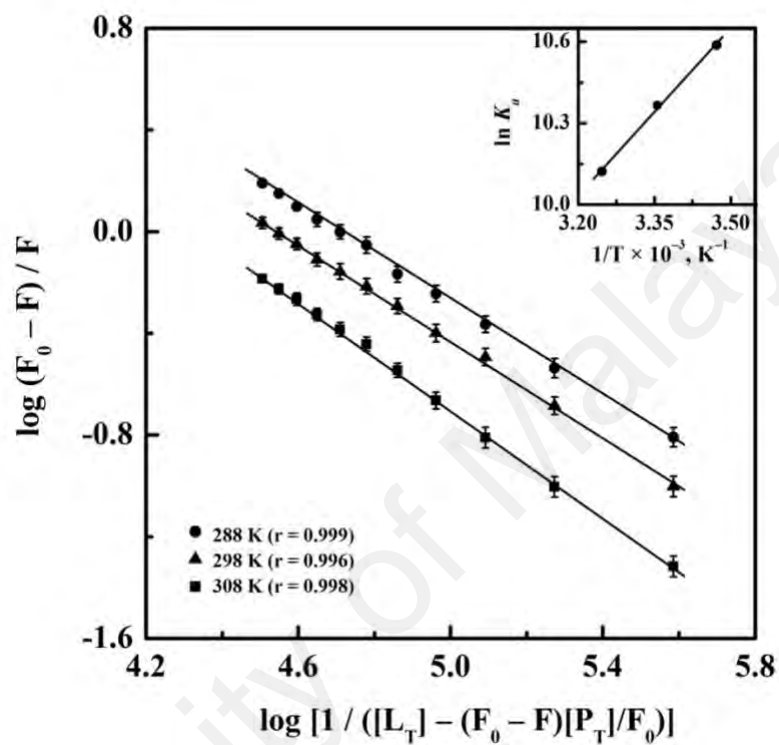
Figure 4.9: Double logarithmic plots for BrdU–HSA system at three different temperatures, *i.e.* 288, 298 and 308 K. Inset shows the van't Hoff plot for BrdU–HSA interaction.

& Subramanian, 1981). Therefore, thermodynamic analysis of BrdU−HSA binding data was made with the help of van't Hoff plot, which is shown as inset of Figure 4.9. The values of the enthalpy change (ΔH) and the entropy change (ΔS) were obtained from the slope and Y-intercept of the van't Hoff plot, while values of the free energy change (ΔG) were calculated using equation (4). Table 4.2 shows these thermodynamic parameters for BrdU−HSA interaction. Negative signs of ΔG and ΔH suggested the binding reaction between BrdU and HSA as spontaneous and exothermic in nature. Decrease in the K_a value with increasing temperature (Table 4.1) was well supported by the exothermic nature of the binding reaction. The sign and magnitude of the thermodynamic parameters predict the interaction forces involved in stabilizing the BrdU−HSA complex. Since both hydrophobic and electrostatic interactions are driven by positive (+ve) entropy change (Ross & Subramanian, 1981), value of ΔS (+28.48 J mol^{-1} K^{-1}), obtained for BrdU−HSA system (Table 4.2) clearly suggested involvement of these forces in the complex stabilization. However, the value of the enthalpy change for electrostatic interactions has been reported to be close to zero (Ross & Subramanian, 1981). The negative (−ve) value of the enthalpy change ($\Delta H = -17.16$ kJ mol^{-1}), obtained for BrdU−HSA system (Table 4.2) ruled out the participation of electrostatic interactions. On the other hand, negative value of ΔH suggested the importance of hydrogen bonds and van der Waals forces in BrdU−HSA complex. Therefore, thermodynamic data suggested involvement of hydrophobic and van der Waals interactions along with hydrogen bonds in the stability of BrdU−HSA complex.

4.2 BrdU-induced structural, microenvironmental and thermal stability changes in HSA

4.2.1 Secondary and tertiary structural changes

Ligand-induced alterations in the protein's secondary structure can be analyzed with the help of the far-UV CD spectra while the near-UV CD spectra are used to monitor

Table 4.2: Thermodynamic parameters of BrdU−HSA system at three different temperatures, as studied in PB 7.4.

T (K)	ΔS (J mol^{-1} K^{-1})	ΔH (kJ mol^{-1})	ΔG (kJ mol^{-1})
288			− 25.36
298	+28.48	−17.16	− 25.65
308			− 25.93

changes in the protein's tertiary structure (Graciani & Ximenes, 2013; Sekowski et al., 2018). Figure 4.10 shows the far-UV CD spectra of HSA (1 μM) in free form as well as upon addition of different BrdU concentrations (1 μM and 3 μM). Emergence of two minima at 211 and 222 nm in the far-UV CD spectrum of HSA (Figure 4.10) indicated dominance of the α-helical structure in the protein. This result was in line with the α-helical nature of HSA (Bozoglan et al., 2014). Although equimolar addition of BrdU showed overlapping CD spectra, increasing the molar ratio of [BrdU]:[HSA] to 3:1 led slight alteration in the far-UV CD spectrum. These results suggested small decrease in the secondary structures of HSA upon complexation with BrdU. Since secondary structures of protein are stabilized by hydrogen bonds (Kelly et al., 2005), slight alteration in the hydrogen bonding network is conceivable upon BrdU binding to HSA.

The near-UV CD spectra of HSA (8 μM) and BrdU–HSA (1:1 and 3:1) mixtures are shown in Figure 4.11. Appearance of two minima around 262 and 269 nm in the near-UV CD spectrum of HSA characterized the tertiary structure of the protein (Wang et al., 2019). Presence of BrdU in the mixture led to alteration in the near-UV CD spectra at both BrdU concentrations (Figure 4.11), which hinted for small tertiary structural changes in the protein upon BrdU addition.

4.2.2 Microenvironmental changes

Three-dimensional (3-D) fluorescence spectroscopy provides information about microenvironmental changes around protein fluorophores under different conditions (Sulkowska, 2002). In view of it, 3-D fluorescence spectra along with contour maps of HSA (3 μM) and BrdU–HSA (3:1) mixture were studied and the results are shown in Figures 4.12 and 4.13, respectively. Peaks 'a' and 'b' are characterized as Rayleigh scattering peaks namely, first order ($\lambda_{ex} = \lambda_{ex}$) and second order ($2\lambda_{ex} = \lambda_{ex}$) scattering peaks, respectively (Zhang et al., 2008). These scattering peaks are commonly observed
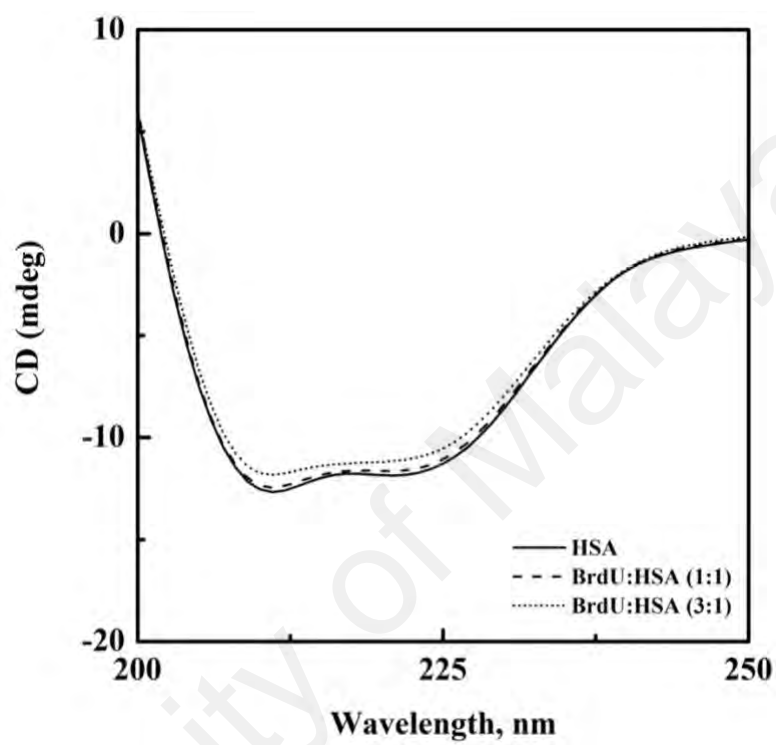
Figure 4.10: Far-UV CD spectra of HSA (1 µM) in the absence and the presence of BrdU in different [BrdU]:[HSA] molar ratios of 1:1 and 3:1, as studied in PB 7.4 at 298 K.
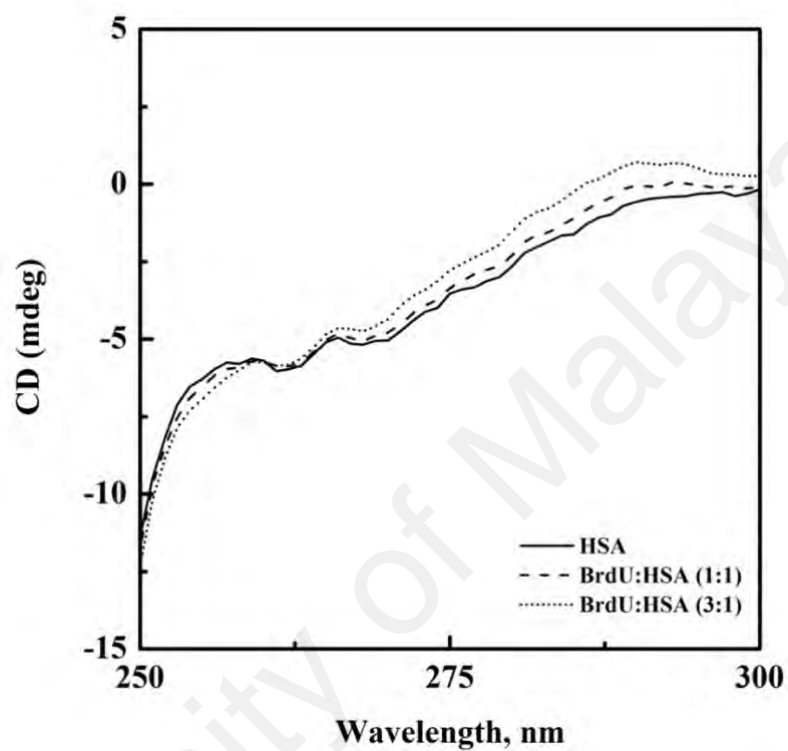
Figure 4.11: Near-UV CD spectra of HSA (8 µM) in the absence and the presence of BrdU in different [BrdU]:[HSA] molar ratios of 1:1 and 3:1, as studied in PB 7.4 at 298 K.
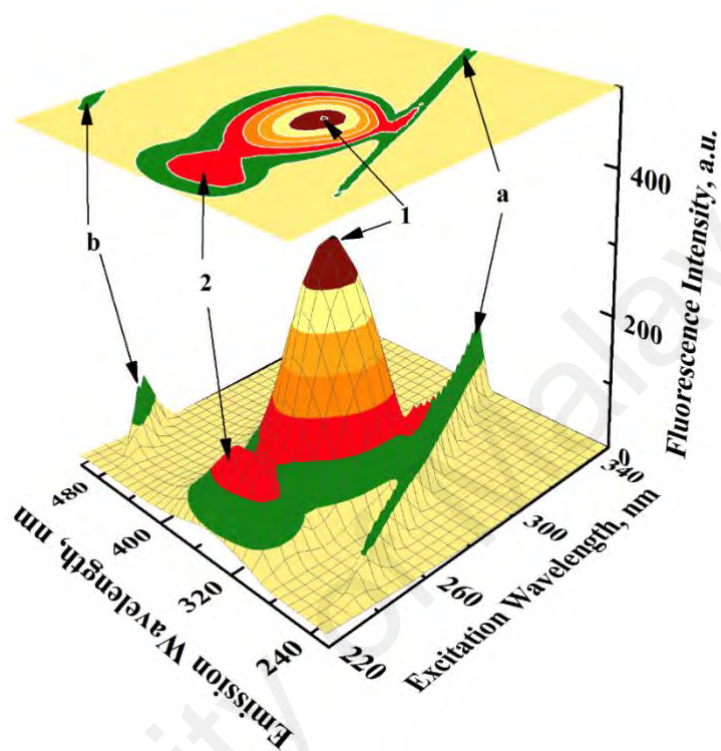
Figure 4.12: Three-dimensional fluorescence spectrum along with contour map of 3 μM HSA, as studied in PB 7.4 at 298 K.
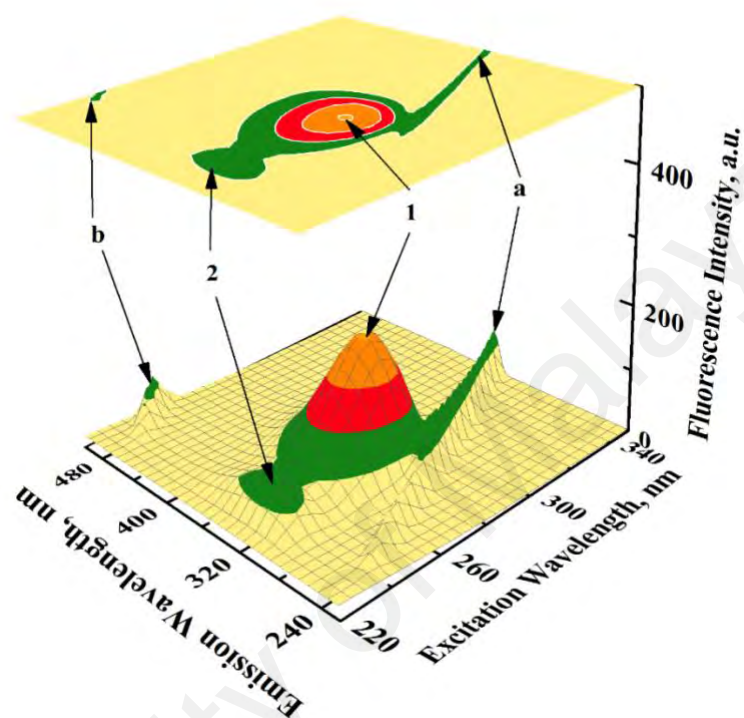
Figure 4.13: Three-dimensional fluorescence spectrum along with contour map of BrdU−HSA mixture (3:1), as studied in PB 7.4 at 298 K.

in the 3-D fluorescence spectra of proteins. Two other peaks, namely, 'peak 1' ($\lambda_{ex} = 280$ nm) and 'peak 2' ($\lambda_{ex} = 230$ nm) represented fluorescence characteristics due to protein fluorophores (Tyr and Trp) (Bortolotti et al., 2016). Tables 4.3 and 4.4 show the analysis of the 3-D fluorescence spectral results of HSA and BrdU−HSA (3:1) mixture, respectively, with respect to the position and fluorescence intensity of each peak. Presence of BrdU in the BrdU−HSA mixture generated significant reduction in the fluorescence intensity of these peaks, being ~50% and ~73% for peaks '1' and '2', respectively (Tables 4.3 and 4.4). In addition to the reduction in the fluorescence intensity, peak '2' also showed a blue shift of 12 nm in the emission maxima. These variations in the fluorescence characteristics of peaks '1' and '2' implied changes in the surrounding microenvironment of protein fluorophores in the presence of BrdU, thus supporting BrdU−HSA complex formation.

4.2.3   Thermal stability changes

To check if the BrdU−HSA complex formation had added to the protein thermal stability (Layton & Hellinga, 2010; Zaroog & Tayyab, 2012; Hoang et al., 2016), thermal denaturation experiments of HSA were conducted in the absence and presence of BrdU, using fluorescence intensity at 343 nm ($FI_{343\ nm}$) as the probe. As noticeable from Figure 4.14, presence of BrdU protected the protein from heat-induced changes in the $FI_{343\ nm}$ to a significant extent at each studied temperature, when compared to those obtained with BrdU-free protein. It is reasonable to believe that formation of BrdU−HSA complex might have added additional forces to the protein as well as protected a little portion of it from heat exposure, thus increased its heat stability. Furthermore, changes in the packing of structural segments of the protein upon ligand binding (Celej et al., 2003) as well as coupling of binding and unfolding equilibria (Shrake & Ross, 1990) may also account for the increased thermal stability of the protein in presence of BrdU. Additionally, increased thermal stability of HSA upon BrdU addition

Table 4.3: Three-dimensional fluorescence spectral characteristics of HSA (3 µM) in PB 7.4 at 298 K.

System	Peak	Peak position λ_{ex} (nm) / λ_{em} (nm)	Intensity
HSA	a	230/230→350/350	17.7→105.6
	b	250/500	91.4
	1	280/337	351.7
	2	230/335	129.8

Table 4.4: Three-dimensional fluorescence spectral characteristics of HSA (3 μM) in the presence of BrdU (9 μM) in PB 7.4 at 298 K.

System	Peak	Peak position λ_{ex} (nm) / λ_{em} (nm)	Intensity
[BrdU]:[HSA]	a	230/230→350/350	19.6→79.8
	b	250/500	65.8
	1	280/336	174.2
	2	230/323	35.0
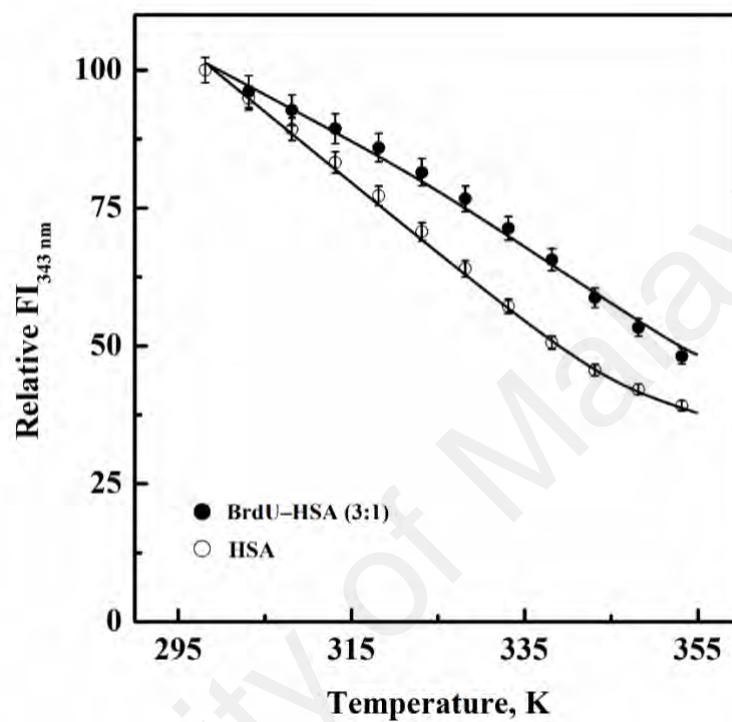
Figure 4.14: Thermal stability profiles of HSA and BrdU−HSA (3:1) mixture in the temperature range of 298−353 K, as studied by fluorescence intensity measurements at 343 nm. The concentrations of HSA and BrdU were 3 μM and 9 μM, respectively.

can also be taken as an indirect evidence of BrdU binding to HSA, as reported in earlier studies (Gonzalez et al., 2000; Ajloo et al., 2007; Sancataldo et al., 2014).

4.3 BrdU binding site characterization

4.3.1 Site marker displacement results

Binding of a majority of ligands to HSA is commonly occurred either at Sudlow's site I (subdomain IIA) or site II (subdomain IIIA) (Sudlow et al., 1975). Therefore, determination of the BrdU-binding site on HSA was made via competitive drug displacement experiments with the help of different site markers, *viz.* WFN and IDN for site I and DZM for site II, employing fluorescence spectroscopy. The fluorescence spectrum of WFN−HSA (1:1) mixture displayed an emission maximum at 383 nm (top spectrum in Figure 4.15) and the spectrum showed a gradual decrease upon addition of increasing BrdU concentrations (spectra 2−12 from top to bottom in Figure 4.15). Fluorescence spectra of 3 μM WFN (spectrum 'a'), 3 μM HSA (spectrum 'b'), Brdu−HSA (11:1) mixture (spectrum 'c') and 33 μM BrdU (spectrum 'd') are also included in Figure 4.15. Except free WFN, showing small but significant fluorescence signal, rest did not produce any significant signal within the studied wavelength range. Progressive decrease in the $FI_{383\ nm}$ with increasing BrdU concentrations, showing 30 % reduction in the $FI_{383\ nm}$ value at 33 μM BrdU concentrations (inset of Figure 4.15) suggested common binding site for WFN and BrdU (Affandi et al., 2017).

To affirm the above finding, experiments with other site marker−HSA complexes (IDN−HSA and DZM−HSA) were performed and the titration results on the relative fluorescence intensities of IDN−HSA and DZM−HSA (1:1) mixtures are displayed Figures 4.16 and 4.17, respectively. Results obtained with HSA alone are also included in these figures for comparison. Although both mixtures showed variation in the extent of decrease in the fluorescence intensity at 343 nm, when compared to that observed with HSA, greater difference was noticed with IDN−HSA mixture than
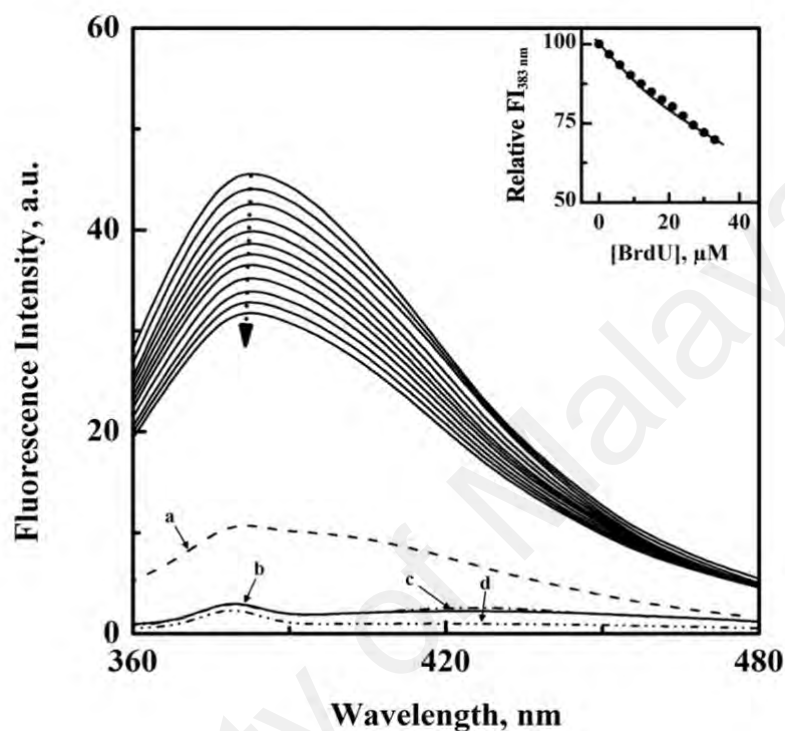
Figure 4.15: Fluorescence spectra of WFN−HSA mixture (3 μM each) with varying concentrations (0−33 μM with 3 μM interval) of BrdU (top to bottom), as studied in PB 7.4 at 298 K. The fluorescence spectra of 3 μM WFN, 3 μM HSA, BrdU−HSA (11:1) mixture and 33 μM BrdU are marked as 'a', 'b', 'c' and 'd', respectively. Inset shows the decrease in the relative $FI_{343\ nm}$ with increasing BrdU concentrations.
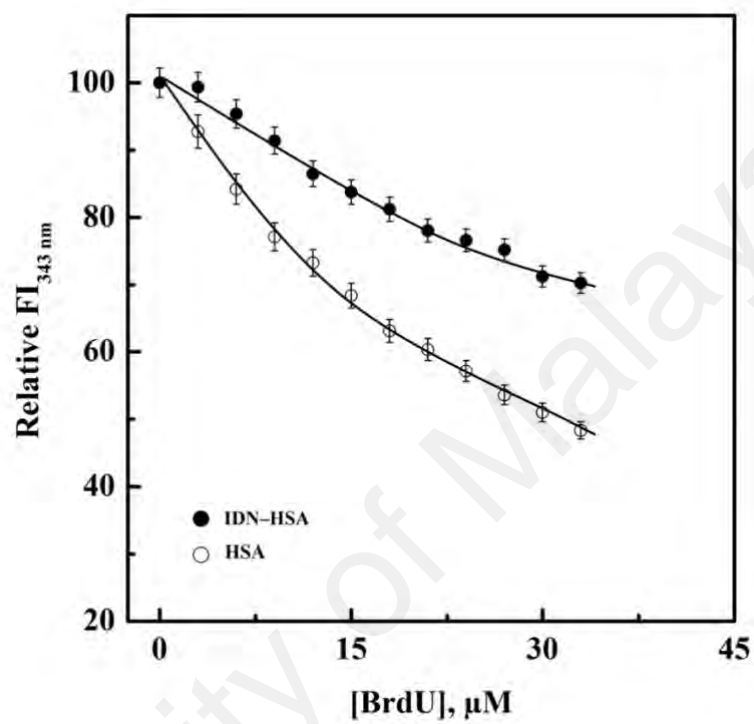
Figure 4.16: Plots showing decrease in the relative $FI_{343\,nm}$ of HSA (3 µM) and IDN−HSA (1:1) mixture (3 µM each) with increasing BrdU concentrations, as studied in PB 7.4 at 298 K.
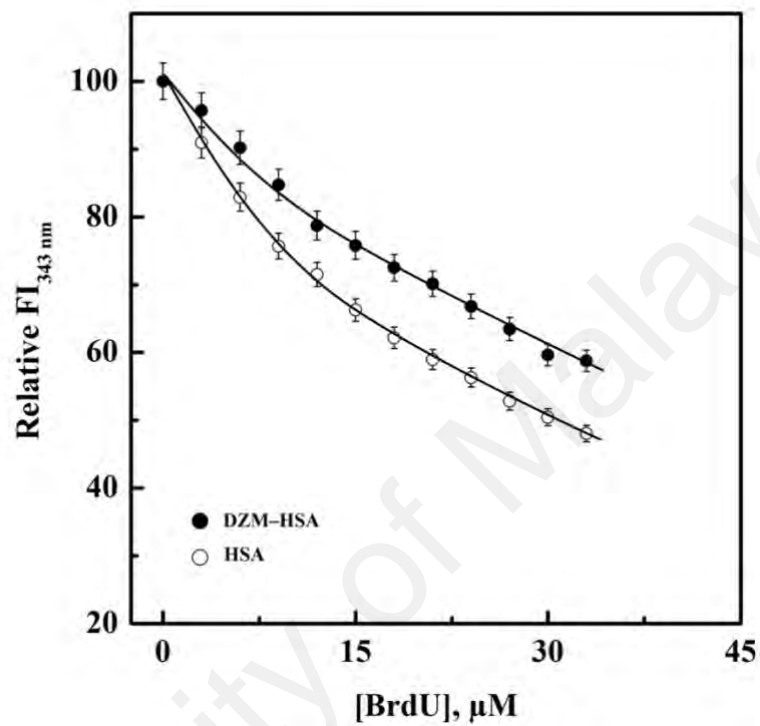
Figure 4.17: Plots showing decrease in the relative $FI_{343\ nm}$ of HSA (3 μM) and DZM−HSA (1:1) mixture (3 μM each) with increasing BrdU concentrations, as studied in PB 7.4 at 298 K.

DZM– HSA mixture, being ~ 20 % and ~ 10 %, respectively at 33 μM BrdU concentration. These observations supported the results obtained with WFN– HSA mixture, thus suggesting site I as the preferred binding site of BrdU on HSA.

4.3.2 Molecular docking analysis

Independent docking simulation enabled the prediction of favourable orientation and interactions of BrdU with HSA binding sites. The cluster analysis of site I exhibited a total of 15 multimember conformational clusters with the highest populated cluster possessing 25 conformations (Figure 4.18). On the other hand, 5 multimember conformational clusters with 84 conformations in the highly populated cluster were seen at site II from 100 docking runs (Figure 4.19). Subsequently, the mean binding energy of the highest populated cluster at site I and site II were found to be –24.39 kJ mol^{-1} (Figure 4.18) and –21.42 kJ mol^{-1} (Figure 4.19), respectively. Moreover, the lowest binding energy at site I and site II were determined as −26.28 kJ mol^{-1} and −22.22 kJ mol^{-1}, respectively. In accordance to the binding energy results stated above, BrdU appeared to have a binding preference for site I compared to site II due to the generation of stronger binding energy.

The binding orientation analyses of the lowest predicted docking energy with favourable interactions between BrdU and binding sites I and II are shown in Figure 4.20 and Figure 4.21, respectively. Four hydrogen bonds were generated between BrdU and HSA at site I (Table 4.5) and BrdU was seen to be enveloped by amino acid residues: Tyr-150, Lys-195, Leu-198, Lys-199, Arg-218, Arg-222, Leu-238, Val-241, His-242, Arg-257, Leu-260, Ser-287, Ile-290, Ala-291 and Glu-292. Presence of 40% hydrophobic residues supported our thermodynamic results about the role of hydrophobic interactions in the stability of BrdU−HSA complex. Although binding of BrdU at site II of HSA also generated four hydrogen bonds (Table 4.6.), yet the binding energy of BrdU at site II (Figure 4.19) was weaker than at site I (Figure 4.18). Thus, it
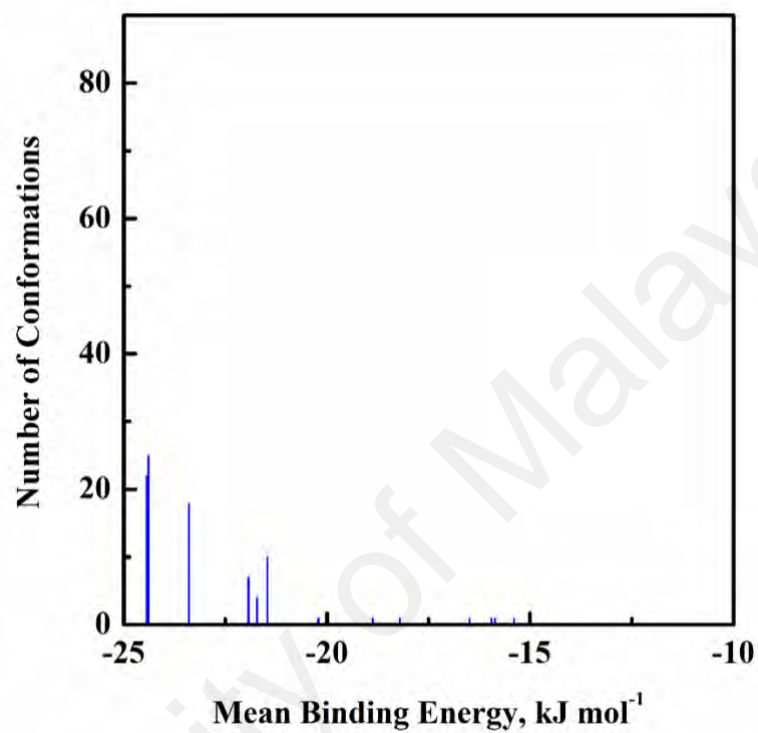
Figure 4.18: Cluster analysis of BrdU−HSA system (100 runs using AutoDock) for the determination of the binding analysis at Sudlow's site I of HSA.
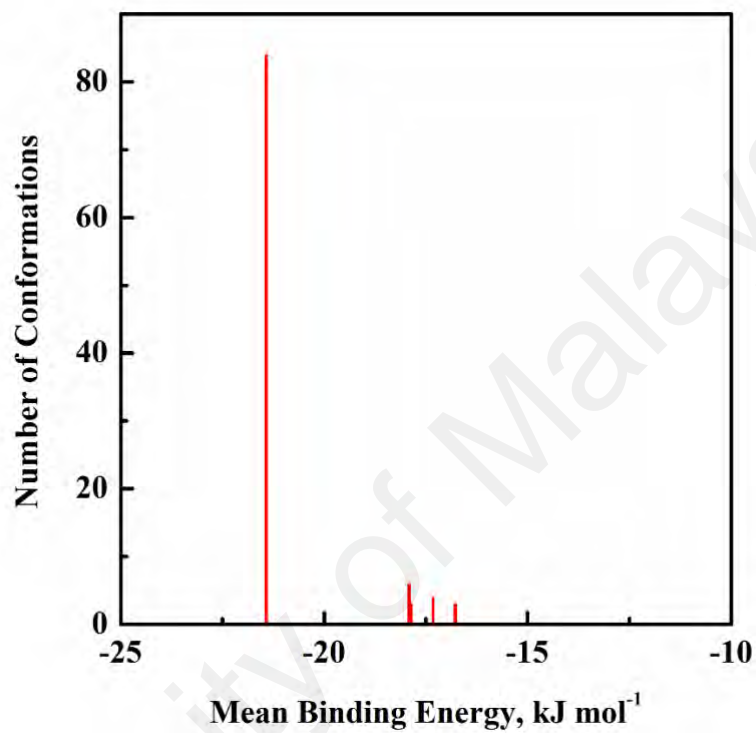
Figure 4.19: Cluster analysis of BrdU−HSA system (100 runs using AutoDock) for the determination of the binding analysis at Sudlow's site II of HSA.
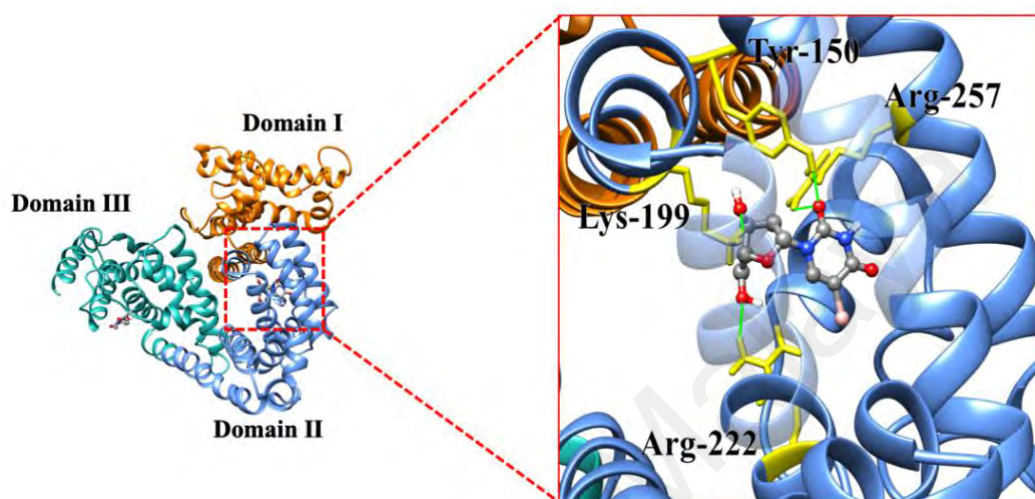
Figure 4.20: Predicted binding orientation of BrdU (ball and stick rendered) on HSA Sudlow's site I, based on the lowest binding energy. Domains I, II and III of HSA are shown in orange, blue and green colours, respectively. The magnified image shows the formation of hydrogen bonds between the amino acid residues of HSA and BrdU at the binding site, located in the subdomain IIA.
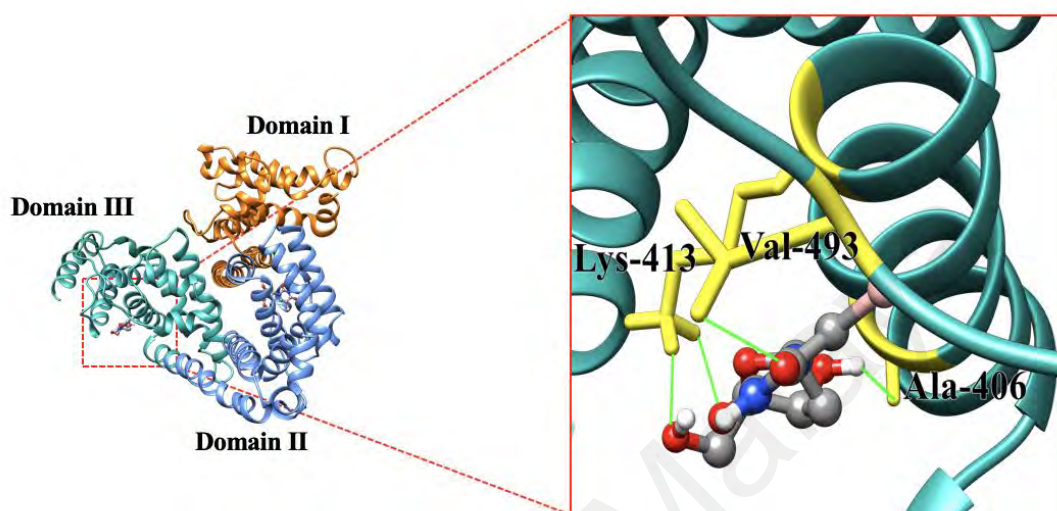
Figure 4.21: Predicted binding orientation of BrdU (ball and stick rendered) on HSA Sudlow's site II, based on the lowest binding energy. Domains I, II and III of HSA are shown in orange, blue and green colours, respectively. The magnified image shows the formation of hydrogen bonds between the amino acid residues of HSA and BrdU at the binding site, located in the subdomain IIIA.

Table 4.5: Distance of hydrogen bond between interacting atoms of the amino acid residues of BrdU at site I of HSA.

HSA binding site	HSA atom	BrdU atom	Distance (Å)
Site I (subdomain IIA)	Tyr-150:HH	O	2.00
	Lys-199:HZ3	O	2.07
	Arg-257: HE	O	2.15
	Arg-222:HH21	O	1.895

Table 4.6: Distance of hydrogen bond between interacting atoms of the amino acid residues of BrdU at site II of HSA.

HSA binding site	HSA atom	BrdU atom	Distance (Å)
	Ala-406: O	O	1.97
Site II	Lys-413: HZ2	O	2.14
(subdomain IIIA)	Lys-413: HZ3	O	1.65
	Val-493: HN	O	2.09

can be suggested that BrdU and HSA form a more stable complex at site I than at site II.

4.4   Metal ion interference

Metal ions play important roles in many biochemical processes and these ions are present in low concentrations in human blood plasma (Guidotti et al., 2008). Therefore, it becomes important to study the effect of these metal ions on the interaction of ligand with plasma proteins. In view of it, influence of some common metal ions such as Ca^{2+}, K^+, Cu^{2+}, Ba^{2+}, Mg^{2+} and Mn^{2+} on BrdU−HSA interaction was investigated in PB 7.4 at 298 K, by determining the binding constant in presence of these ions. Table 4.7 shows the values of the binding constant (K_a) of BrdU−HSA interaction in the absence and presence of these metal ions (30 μM). As evident from Table 4.7, K_a value showed smaller but significant decrease in the presence of these metal ions following the order: K^+/ Mn^{2+} < Cu^{2+} < Ba^{2+} < Mg^{2+}. On the other hand, a smaller but significant increase in the K_a value was noticed in the presence of Ca^{2+}. These results suggested metal ions' interference with BrdU−HSA complex formation, as revealed by the change in the binding affinity in the presence of metal ions. Such intrusion may reduce or lengthen the storage time of the drug in blood plasma that could weaken or increase the efficiency of the drug (Cui et al., 2004; Cheng et al., 2013). Hence, the presence of Ca^{2+} helps in facilitating BrdU−HSA complex, thus lengthens the storage time of BrdU in blood plasma and increases its efficacy.

Table 4.7: Values of the binding constant (K_a) of BrdU–HSA interaction in the absence and the presence of different metal ions (30 µM), as studied in PB 7.4 at 298 K.

Metal ion	$K_a \times 10^4$ (M^{-1})
-	3.18 ± 0.17
Ca^{2+}	4.26 ± 0.39
Cu^{2+}	2.22 ± 0.04
K^{2+}	2.89 ± 0.01
Ba^{2+}	2.13 ± 0.01
Mg^{2+}	1.50 ± 0.12
Mn^{2+}	2.85 ± 0.09

CHAPTER 5: CONCLUSION

Interaction between BrdU and HSA was asserted from the fluorescence quenching titration and absorption spectral results. BrdU−HSA complex was stabilized by hydrophobic and van der Waals interactions along with hydrogen bonds. BrdU addition to the protein produced alteration in the secondary and tertiary structures including microenvironmental variations around Tyr and Trp residues. BrdU seems to form a complex with the protein after binding at Sudlow's site I (subdomain IIA) and formation of this complex added to the protein's thermal stability. Influence of a few metal ions, (Ca^{2+}, K^+, Cu^{2+}, Ba^{2+}, Mg^{2+} and Mn^{2+}) on BrdU−HSA interaction was also noticed. These findings would be helpful in understanding the pharmacokinetics of BrdU in human circulation.

REFERENCES

Abou-Zied, O. K., & Al-Shihi, O. I. (2008). Characterization of subdomain IIA binding site of human serum albumin in its native, unfolded, and refolded states using small molecular probes. *Journal of the American Chemical Society, 130*, 10793–10801.

Adema, A. D., Radi, M., Narayanasamy, J., Hoebe, E. K., Alexander, L. E., Chu, C. K., & Peters, J. (2007). Troxacitabine prodrugs for pancreatic cancer. *Nucleosides, Nucleotides & Nucleic Acids, 26*, 1073–1077.

Affandi, I. S. M., Lee, W. Q., Feroz, S. R., Mohamad, S. B., & Tayyab, S. (2017). Interaction of stattic, a STAT3 inhibitor with human serum albumin: Spectroscopic and computational study. *Journal of Biomolecular Structure and Dynamics, 35*, 3581−3590.

Agrawal, R., Thakur, Y., Tripathi, M., Siddiqi, M. K., Khan, R. H., & Pande, R. (2019). Elucidating the binding propensity of naphthyl hydroxamic acid to human serum albumin (HSA): Multi-spectroscopic and molecular modeling approach. *Journal of Molecular Structure, 1184*, 1–11.

Ajloo, D., Benham, H., Saboury, A. A., Mohamadi-Zonoz, F., Ranjbar, B., Moosavi-Movahedi, A. A., … Amani, M. (2007). Thermodynamic and structural studies on the human serum albumin in the presence of a polyoxometalate. *Bulletin of the Korean Chemical Society, 28*, 730–736.

Amrutkar, M., & Gladhaug, I. P. (2017). Pancreatic cancer chemoresistance to gemcitabine. *Cancers, 9*, 1–23.

Barre, L., Hovhannisyan, N., Bodet-Milin, C., Kraeber-Bodere, F., & Damaj, G. (2019). [^{18}F]-Fludarabine for hematological malignancies. *Frontiers in Medicine, 6*, 1–5.

Barta, J. A., Powell, C. A., & Wisnivesky, J. P. (2019). Global epidemiology of lung cancer. *Annals of Global Health, 85*, 1−16.

Barua, A., Choudhury, P., Maity, J. K., Mandal, S. B., Mandal, S., & Saha, P. (2019). Chemotherapeutic potential of novel non-toxic nucleoside analogues on EAC ascitic tumour cells. *Free Radical Research, 53*, 57–67.

Baskar, R., Lee, K. A., Yeo, R., & Yeoh, K-W. (2012). Cancer and radiation therapy: Current advances and future directions. *International Journal of Medical Sciences, 9*, 193−199.

Bayo, J., Molina, R., Perez, J., Perez-Ruiz, E., Aparicio, J., Beato, C., … Santaballa, A. (2019). SEOM clinical guidelines to primary prevention of cancer (2018). *Clinical and Translational Oncology, 21*, 106−113.

Bell, K. L., & Brenner, H. C. (1982). Phosphorescence and optically detected magnetic resonance study of the tryptophan residue in human serum albumin. *Biochemistry, 21*, 799−804.

Bertani, E., Chiappa, A., Biffi, R., Bianchi, P. P., Radice, D., Branchi, V., … Andreoni, B. (2011). Assessing appropriateness for elective colorectal cancer surgery: Clinical, oncological, and quality-of-life short-term outcomes employing different treatment approaches. *International Journal of Colorectal Disease, 26*, 1317−1327.

Bhattacharya, A. A., Curry, S., & Franks, N. P. (2000). Binding of the general anesthetics propofol and halothane to human serum albumin. High resolution crystal structures. *The Journal of Biological Chemistry, 275*, 38731–38738.

Bi, S., Ding, L., Tian, Y., Song, D., Zhou, X., Liu, X., & Zhang, H. (2004). Investigation of the interaction between flavonoids and human serum albumin. *Journal of Molecular Structure, 703*, 37–45.

Bian, Z., Jin, L., Zhang, J., Yin, Y., Quan, C., Hu, Y., … Huang, Z. (2016). LncRNA—UCA1 enhances cell proliferation and 5-fluorouracil resistance in colorectal cancer by inhibiting miR-204-5p. *Scientific Reports, 6*, 1–12.

Bortolotti, A., Wong, Y. H., Korsholm, S. S., Bahring, N. H. B., Bobone, S., Tayyab, S., … Stella. L. (2016). On the purported "backbone fluorescence" in protein three-dimensional fluorescence spectra. *RSC Advances, 6*, 112870−112876.

Bozoglan, B. K., Tunc, S., & Duman, O. (2014). Investigation of neohesperidin dihydrochalcone binding to human serum albumin by spectroscopic methods. *Journal of Luminescence, 155*, 198–204.

Bray, F., Ferlay, J., Soerjomataram, I., Siegel, R. L., Torre, L. A., & Jemal, A. (2018). Global cancer statistics 2018: GLOBOCAN estimates of incidence and mortality worldwide for 36 cancers in 185 countries. *CA: A Cancer Journal for Clinicians, 68*, 394−424.

Cano-Soldado, P., & Pastor-Anglada, M. (2011). Transporters that translocate nucleosides and structural similar drugs: Structural requirements for substrate recognition. *Medicinal Research Reviews, 32*, 428–457.

Carlini, F., Ridolfi, B., Molinari, A., Parisi, C., Bozzuto, G., Toccacieli, L., … Gaudi, S. (2010). The reverse transcription inhibitor abacavir shows anticancer activity in prostate cancer cell lines. *PloS ONE, 5*, Article# e14221.

Carlotto, A., Hogsett, V. L., Maiorini, E. M., Razulis, J. G., & Sonis, S. T. (2013). The economic burden of toxicities associated with cancer treatment: Review of the literature and analysis of nausea and vomiting, diarrhoea, oral mucositis and fatigue. *PharmacoEconomics, 31*, 753–766.

Carter, D. C., & Ho, J. X. (1994). Structure of serum albumin. *Advances in Protein Chemistry, 45*, 153–203.

Cavanagh, B. L., Walker, T., Norazit, A., & Meedeniya, A. C. B. (2011). Thymidine analogues for tracking DNA synthesis. *Molecules, 16*, 7980–7993.

Celano, M., Calvagno, M. G., Bulotta, S., Paolino, D., Arturi, F., Rotiroti, D., … Russo, D. (2004). Cytotoxic effects of gemcitabine-loaded liposomes in human anaplastic thyroid carcinoma cells. *BMC Cancer, 4*, 1–5.

Celej, M. S., Montich, G. G., & Fidelio, G. D. (2003). Protein stability induced by ligand binding correlates with changes in protein flexibility. *Protein Science, 12*, 1496–1506.

Cheng, Z., Liu, R., & Jiang, X. (2013). Spectroscopic studies on the interaction between tetrandrine and two serum albumins by chemometrics methods. *Spectrochimica Acta Part A: Molecular and Biomolecular Spectroscopy, 115*, 92–105.

Chuang, V. T., & Otagiri, M. (2001). Flunitrazepam, a 7-nitro-1,4-benzodiazepine that is unable to bind to the indole-benzodiazepine site of human serum albumin. *Biochimica et Biophysica Acta – Protein Structure and Molecular Enzymology, 1546*, 337–345.

Crane, A. M., & Bhattacharya, S. K. (2013). The use of bromodeoxyuridine incorporation assays to assess corneal stem cell proliferation. *Corneal Regenerative Medicine, 1014*, 65–70.

Cui, F. L., Fan, J., Li, J. P., & Hu, Z. (2004). Interactions between 1-benzoyl-4-p-chlorophenyl thiosemicarbazide and serum albumin: Investigation by fluorescence spectroscopy. *Bioorganic and Medicinal Chemistry, 12*, 151–157.

Dabkowska, M., Adamczyck, Z., & Kujda, M. (2013). Mechanism of HSA adsorption on mica determined by streaming potential, AFM and XPS measurements. *Colloids and Surfaces. B, Biointerfaces, 101*, 442–449.

Diab, R., Degobert, G., Hamoudeh, M., Dumontet, C., & Fessi, H. (2007). Nucleoside analogue delivery systems in cancer therapy. *Expert Opinion Drug Delivery, 4*, 513–531.

Diermeir, S., Schmidt-Bruecken, E., Kubbies, M., Kunz-Schughart, L. A., & Brockhoff, G. (2004). Exposure to continuous bromodeoxyuridine (BrdU) differentially affects cell cycle progression of human breast and bladder cancer cell lines. *Cell Proliferation, 37*, 195–206.

Dockal, M., Carter, D. C., & Ruker, F. (1999). The three recombinant domains of human serum albumin: Structural characterization and ligand binding properties. *The Journal of Biological Chemistry, 274*, 29303–29310.

Dugaiczyk, A., Law, S. W., & Dennison, O. E. (1982). Nucleotide sequence and the encoded amino acids of human serum albumin mRNA. *Proceedings of the National Academy of Sciences, USA, 79*, 71−75.

El Kadi, N., Taulier, N., Le-Huerou, J. Y., Gindre, M., Urbach, W., Nwigwe, I., … Waks, M. (2006). Unfolding and refolding of bovine serum albumin at acid pH: Ultrasound and structural studies. *Biophysical Journal, 9*, 3397−3404.

Eyer, L., Nechka, R., Clercq, E., Seley-Radtke, K., & Ruzek, D. (2018). Nucleosides analogs as a rich source of antiviral agents active against arthropod-borne flaviviruses. *Antiviral Chemistry and Chemotherapy, 26*, 1−28.

Fehske, K. J., Schlafer, U., Wollert, U., & Muller, W. E. (1982). Characterization of an important drug binding area on human serum albumin including the high-affinity binding sites of warfarin and azapropazone. *Molecular Pharmacology, 21*, 387–393.

Feroz, S. R., Mohamad, S. B., Lee, G. S., Malek, S. N. A., & Tayyab, S. (2015). Supramolecular interaction of 6-shogaol, a therapeutic agent of *Zingiber officinale* with human serum albumin as elucidated by spectroscopic, calorimetric and molecular docking methods. *Phytomedicine, 22*, 621–630.

Ferrer, M. L., Duchowicz, R., Carrasco, B., Torre, J. G., & Acuna, A. U. (2001). The conformation of serum albumin in solution: A combined phosphorescence depolarization-hydrodynamic modeling study. *Biophysical Journal, 80*, 2422–2430.

Figge, J., Rossing, T. H., & Fencl, V. (1991). The role of serum proteins in acid-base equilibria. *Journal of Laboratory and Clinical Medicine, 117*, 453–467.

Fu, L., Liu, X. F., Zhou. Q. X., Zhang, J. X., Dong, J. Y., & Wang, J. F. (2014). Characterization of the interactions of human serum albumin (HSA), gatifloxacin, and metronidazole using spectroscopic and electrochemical methods. *Journal of Luminescence, 149*, 208–214.

Fung, J., Lai, C-L., Seto, W-K., & Yuen, M-F. (2011). Nucleoside/nucleotide analogues in the treatment of chronic hepatitis B. *Journal of Antimicrobial Chemotherapy, 66*, 2715–2725.

Galmarini, C. M., Mackey, J. R., & Dumontet, C. (2002). Nucleoside analogues and nucleobases in cancer treatment. *The Lancet Oncology, 3*, 415−424.

Gan, N., Sun, Q., Tang, P., Wu, D., Xie, T., Zhang, Y., & Li, H. (2019). Determination of interactions between human serum albumin and niraparib through multi-spectroscopic and computational methods. *Spectrochimica Acta Part A: Molecular and Biomolecular Spectroscopy, 206*, 126–134.

Genini, D., Adachi, S., Chao, Q., Rose, D. W., Carrera, C. J., Cottam, H. B., … Leoni, L. M. (2000). Deoxyadenosine analogs induce programmed cell death in chronic lymphocytic leukemia cells by damaging the DNA and by directly affecting the mitochondria. *Blood, 96*, 3537–3543.

Ghuman, J., Zunszain, P. A., Petitpas, I., Bhattacharya, A. A., Otagiri, M., & Curry, S. (2005). Structural basis of the drug-binding specificity of human serum albumin. *Journal of Molecular Biology, 353*, 38–52.

Gianazza, E., Frigerio, A., Astrua-Testori, S., & Righetti, P. G. (1984). The behavior of serum albumin upon isoelectric focusing on immobilized pH gradients. *Electrophoresis, 5*, 310−312.

Gonzalez, M, Argarana, C., & Fidelio, G. (2000). Extremely high thermal stability of streptavidin and avidin upon biotin binding. *Biomolecular Engineering, 16*, 67–72.

Graciani, F., & Ximenes, V. (2013). Investigation of human albumin-induced circular dichroism in dansylglycine. *PLoS ONE, 8*, Article# e76849.

Guidotti, T. L., McNamara, J., & Moses, M. S. (2008). The interpretation of trace element analysis in body fluids. *Indian Journal of Medical Research, 128*, 524– 532.

Halgren, T. A. (1996). Merck molecular force field. I. Basis, form, scope, parameterization, and performance of MMFF9. *Journal of Computational Chemistry, 17*, 490–519.

Hanwell, M. D., Curtis, D. E., Lonie, D. C., Vandermeersch, T., Zurek, E., & Hutchison, G. R. (2012). Avogadro: An advanced semantic chemical editor, visualization, and analysis platform. *Journal of Cheminformatics, 4*, 1–17.

Haye-Bertolozzi, J. E., & Aparicio, O. M. (2018). Quantitative bromodeoxyuridine immunoprecipitation analyzed by high-throughput sequencing (qBrdU-Seq or QBU). *Methods in Molecular Biology, 1672*, 209–225.

He, X. M., & Carter, D. C. (1992). Atomic structure and chemistry of human serum albumin. *Nature, 358*, 209–215.

Hill, B., Tsuboi, A., & Baserg, R. (1974). Effect of 5-bromodeoxyuridine on chromatin transcription in confluent fibroblasts. *Proceedings of the National Academy of Sciences, USA, 71*, 455–459.

Hoang, H., Manyanga, F., Morakinyo, M. K., Pinkert, V., Sarwary, F., Fish, D. J., … Benight, A. S. (2016). Effects of selective biotinylation on the thermodynamic stability of human serum albumin. *Journal of Biophysical Chemistry, 7*, 9–29.

Hosokawa, M., Tanaka, S., Ueda, K., Iwakawa, S., & Ogawara, K-I. (2019). Decitabine exerted synergistic effects with oxaliplatin in colorectal cancer cells with intrinsic resistance to decitabine. *Biochemical and Biophysical Research Communications, 509*, 249–254.

Hu, Y. J., Ou-Yang, Y., Dai, C. M., Liu, Y., & Xiao, X. H. (2010). Site-selective binding of human serum albumin by palmatine: Spectroscopic approach. *Biomacromolecules, 11*, 106–112.

Hunter, M. J., & Mcduffie, F. C. (1959). Molecular weight studies on human serum albumin after reduction and alkylation of disulfide bonds. *Journal of the American Chemical Society, 81*, 1400–1406.

Ismail, M. K., Armstrong, K. A., Hodder, S. L., Horswell, S. L., Male, L., Nguyen, H. V., … Tucker, J. H. R. (2020). Organometallic nucleoside analogues: Effect of the metallocene metal atom on cancer cell line toxicity. *Dalton Transactions, 49*, 1181–1190.

Jagarlamudi, K. K., & Shaw, M. (2018). Thymidine kinase 1 as a tumor biomarker: Technical advances offer new potential to an old biomarker. *Biomarkers in Medicine, 12*, 1035–1048.

Jordheim, L. P., Durantel, D., Zoulim, F., & Dumontet, C. (2013). Advances in the development of nucleoside and nucleotide analogues for cancer and viral diseases. *Nature Reviews Drug Discovery, 12*, 447–464.

Kabir, M. Z., Tee, W. V., Mohamad, S. B., Alias, Z., & Tayyab, S. (2017). Comprehensive insight into the binding of sunitinib, a multi-targeted anticancer drug to human serum albumin. *Spectrochimica Acta Part A: Molecular and Biomolecular Spectroscopy, 181*, 254–263.

Kabir, M. Z., Tee, W. V., Mohamad, S. B., Alias, Z., & Tayyab, S. (2016). Interaction of an anticancer drug, gefitinib with human serum albumin: Insights from fluorescence spectroscopy and computational modeling analysis. *RSC Advances, 6*, 91756–91767.

Kallubai, M., Reddy, S. P., Dubey, S., Ramachary, D. B., & Subramanyam, R. (2018). Spectroscopic evaluation of synthesized 5β-dihydrocortisol and 5β-dihydrocortisol acetate binding mechanism with human serum albumin and their role in anticancer activity. *Journal of Biomolecular Structure and Dynamics, 37,* 623–640.

Kelly, S. M., Jess, T. J., & Price, N. C. (2005). How to study proteins by circular dichroism. *Biochimica et Biophysica Acta, 1751*, 119–139.

Khanna, N. C., Tokuda, M., & Waisman, D. M. (1986). Conformational changes induced by binding of divalent cations to calregulin. *The Journal of Biological Chemistry, 261*, 8883–8887.

Kim, R. D., Alberts, S. R., Pena, C., Genvresse, I., Ajavon-Hartmann, A., Xia, C., … Grilley-Olson, J. E. (2018). Phase I dose-escalation study of copanlisib in combination with gemcitabine or cisplatin plus gemcitabine in patients with advanced cancer. *British Journal of Cancer, 118*, 462–470.

Korolenko, E. A., Korolik, E. V., Korolik, A. K., & Kirkovskii, V. V. (2007). Estimation of the binding ability of main transport proteins of blood plasma with liver cirrhosis by the fluorescent probe method. *Journal of Applied Spectroscopy, 74*, 561–566.

Kragh-Hansen, U. (1988). Evidence for a large and flexible region of human serum albumin possessing high affinity binding sites for salicylate, warfarin, and other ligands. *Molecular Pharmacology, 34*, 160–171.

Kragh-Hansen, U. (1990). Structure and ligand binding properties of human serum albumin. *Danish Medicinal Bulletin, 37*, 57–84.

Kragh-Hansen, U., Chuan, V. T. G., & Otagiri, M. (2002). Practical aspects of the ligand binding and enzymatic properties of human serum albumin. *Biological and Pharmaceutical Bulletin, 25*, 695–704.

Krainer, M. (2003). Efficacy of combination therapy versus monotherapy. *Breast Cancer Research and Treatment, 81*, S11–S15.

Kuhn, H. G., & Cooper-Kuhn, C. M. (2007). Bromodeoxyuridine and the detection of neurogenesis. *Current Pharmaceutical Biotechnology, 8*, 127−131.

Laakmann, E., Witzel., & Muller, V. (2017). Efficacy of liposomal cytarabine in the treatment of leptomeningeal metastasis of breast cancer. *Breast Care, 12,* 165–167.

Lakowicz, J. R. (2006). Principles of Fluorescence Spectroscopy (3rd edn.). *New York, Springer.*

Lapponi, M. J., Rivero, C. W., Zinni, M. A., Britos, C. N., & Trelles, J. A. (2016). New developments in nucleoside analogues biosynthesis: A review. *Journal of Molecular Catalysis B: Enzymatic, 133*, 218–233.

Layton, C. J., & Hellinga, H. W. (2010). Thermodynamic analysis of ligand-induced changes in protein thermal unfolding applied to high-throughput determination of ligand affinities with extrinsic fluorescent dyes. *Biochemistry, 49*, 10831–10841.

Lengronne, A., Pasero, P., Bensimon, A., & Schwob, E. (2001). Monitoring S phase progression globally and locally using BrdU incorporation in TK+ yeast strains. *Nucleic Acids Research, 7*, 1433−1442.

Levkoff, L. H., Marshall, G. P., Ross, H. H., Caldeira, M., Reynolds, B. A., Cakiroglu, M., … Laywell, E. D. (2008). Bromodeoxyuridine inhibits cancer cell proliferation *in vitro* and *in vivo*. *Neoplasia, 10*, 804−816.

Lindup, W. E., & Orme, M. C. (1981). Clinical pharmacology: Plasma protein binding of drugs. *British Medical Journal, 282*, 212–214.

Lloveras, B., Edgerton, S., & Thor, A. D. (1991). Evaluation of *in vitro* bromodeoxyuridine labeling of breast carcinomas with the use of a commercial kit. *American Journal of Clinical Pathology, 95,* 41–47.

Lubecka, K., Kaufman-Szymczyk, A., Cebula-Obrzut, B., Smolewski, P., Szemraj, J., & Fabianowska-Majewska, K. (2018). Novel clofarabine-based combinations with polyphenols epigenetically reactivate retinoic acid receptor beta, inhibit cell growth, and induce apoptosis of breast cancer cells. *International Journal of Molecular Sciences, 19,* 1–23.

Manjushree, M., & Revanasiddappa, H. D. (2019). Interpretation of the binding interaction between bupropion hydrochloride with human serum albumin: A collective spectroscopic and computational approach. *Spectrochimica Acta Part A: Molecular and Biomolecular Spectroscopy, 209*, 264–273.

Mansson, E., Flordal, E., Liliemark, J., Spasokoukotskaja, T., Elford, H., Lagercrantz, … Albertioni, F. (2003). Down-regulation of deoxycytidine kinase in human leukemic cell lines resistant to cladribine and clofarabine and increased

ribonucleotide reductase activity contributes to fludarabine resistance. *Biochemical Pharmacology, 65*, 237–247.

Mathew, P., Yang, J., Kim, S. J., Fidler, I., Bucana, C., Troncoso, P., … Thall, C. (2004). Inhibition of functional osteoblasts with the platelet-derived growth factor receptor (PDGFR) inhibitor imatinib mesylate in androgen- independent prostate cancer (PCa). *Journal of Clinical Oncology, 22*, 4625– 4625.

Minghetti, P. P., Ruffner, D. E., Kuang, W. J., Dennison, O. E., Hawkins, J. W., Beattie, … Dugaiczyk, A. (1986). Molecular structure of the human albumin gene is revealed by nucleotide sequence within q11-22 of chromosome 4. *The Journal of Biological Chemistry, 261*, 6747−6757.

Mingqiang, L., Lao, Y-H., Mintz, R. L.R., Chen, Z., Shao, D., Hu, H., … Leong, K. W. (2019). A multifunctional mesoporous silica–gold nanocluster hybrid platform for selective breast cancer cell detection using a catalytic amplification-based colorimetric assay. *Nanoscale, 11*, 2631−2636.

Minuesa, G., Huber-Ruano, I., Pastor-Anglada, M., Koepsell, H., Clotet, B., & Martinez-Picado, J. (2011). Drug uptake transporters in antiretroviral therapy. *Pharmacology and Therapeutics, 132*, 268–279.

Moog, R., Burger, A., Brandl, M., Schuler, J. Schubert, R. Unger, C. … Massing, U. (2002). Change in pharmacokinetic and pharmacodynamic behavior of gemcitabine in human tumor xenografts upon entrapment in vesicular phospholipid gels. *Cancer Chemotherapy and Pharmacology, 49*, 356–366.

Morris, G. M., Huey, R., Lindstrom, W., Sanner, M. F., Belew, R. K., Goodsell, D. S., & Olson, A. J. (2009). Autodock4 and AutoDockTools4: Automated docking with selective receptor flexibility. *Journal of Computational Chemistry, 30*, 2785–2791.

Mothi. N., Muthu. S. A., Kale. A., & Ahmad. B. (2005). Curcumin promotes fibril formation in F isomer of human serum albumin via amorphous aggregation. *Biophysical Chemistry, 207*, 30–39.

Mottini, C., Tomihara, H., Carella, D., Lamolinara, A., Iezzi, M., Huang, J. K., … Cardone, L. (2019). Predictive signatures inform the effective repurposing of decitabine to treat KRAS-dependent pancreatic ductal adenocarcinoma. *Cancer Research, 79*, 5612–5625.

Nagati, V., Kallubai, M., Chinthapalli, D. J., & Subramanyam, R. (2018). Exploration of binding studies of β-Oxalyldiamino propionic acid (β-ODAP) a non-protein amino acid with human serum albumin-biophysical and computational approach. *Journal of Biomolecular Structure and Dynamics, 37,* 3914–3922.

Nakamura, S., Takeda, Y., Kanno, M., Yoshida, T., Ohtake, S., Kobayashi, K., … Matsuda, T. (1991). Application of bromodeoxyuridine (BrdU) and anti-BrdU monoclonal antibody for the *in vivo* analysis of proliferative characteristics of human leukemic cells in bone marrows. *Oncology, 48*, 285−289.

Nicholson, J. P., Wolmarans, M. R., & Park, G. R. (2000). The role of albumin in critical illness. *British Journal of Anaesthesia, 85*, 599–610.

Olson, R. E., & Christ, D. D. (1996). Plasma protein binding to drugs. *Annual Reports in Medicinal Chemistry, 31*, 327–336.

Painter, L., Harding, M. M., & Beeby, P. J. (1998). Synthesis and interaction with human serum albumin of the first 3,18-disubstituted derivative of bilirubin. *Journal of Chemical Society, Perkin Transactions 1, 18*, 3041–3044.

Park, S-S., Park, S-K., Lim J-H., Choi, Y-H., Kim, W-J., & Moon, S-K. (2011). Esculetin inhibits cell proliferation through the Ras/ERK1/2 pathway in human colon cancer cells. *Oncology Reports, 25*, 223−230.

Paus, R., Haslam, I. S., Sharov, A. A., & Botchkarev, V. A. (2013). Pathobiology of chemotherapy-induced hair loss. *The Lancet Oncology, 14*, e50−e59.

Perez-Zamorano, B., & Valverde-Garduno, V. (2015). Immune challenge induces DNA synthesis and nuclear fragmentation in *Aedes aegypti* fat body cells. *International Journal of Mosquito Research, 2*, 24–28.

Perigaud, C., Gosselin, G., & Imbach J. L. (1992). Nucleoside analogues as chemotherapeutic agents: A review. *Nucleosides and Nucleotides, 11*, 903–945.

Peters, T., Jr. (1996). All About Albumin: Biochemistry, Genetics, and Medical Applications. *San Diego: Academic Press.*

Pettersen, E. F., Goddard, T. D., Huang, C. C., Couch, G. S., Greenblatt, D. M., Meng, E. C., & Ferrin, T. E. (2004). UCSF Chimera − A visualization system for exploratory research and analysis. *Journal of Computational Chemistry, 25*, 1605–1612.

Port, R. E., Schuster, C., Port, C. R., & Bachert, P. (2006). Simultaneous sustained release of fludarabine monophosphate and Gd-DTPA from an interstitial liposome depot in rats: Potential for indirect monitoring of drug release by magnetic resonance imaging. *Cancer Chemotherapy and Pharmacology, 58*, 607–617.

Pridgeon, S. W., Heer, R., Taylor, G. A., Newell, D. R., O'Toole, K., Robinson, M., … Boddy, A. V. (2011). Thiothymidine combined with UVA as a potential novel therapy for bladder cancer. *British Journal of Cancer, 104*, 1869–1876.

Putnam, F. W. (1975). The Plasma Proteins (2nd ed.). *New York: Academic Press.*

Quinlan, G. J., Martin, G. S., & Evans, T. W. (2005). Albumin: Biochemical properties and therapeutic potential. *Hepatology, 41*, 1211–1219.

Rades, D., Seidl, D., Janssen, S., Bajrovic, A., Karner, K., Strojan, P., & Schild, S. E. (2016). Comparison of weekly administration of cisplatin versus three courses of cisplatin 100 mg/m^2 for definitive radiochemotherapy of locally advanced head-and-neck cancers. *BMC Cancer, 16*, 1–8.

Rompay, A. R. V., Johansson, M., & Karlsson, A. (2000). Phosphorylation of nucleosides and nucleoside analogs by mammalian nucleoside monophosphate kinases. *Pharmacology and Therapeutics, 87*, 189–198.

Ross, P. D., & Subramanian, S. (1981). Thermodynamics of protein association reactions: Forces contributing to stability. *Biochemistry, 20*, 3096–3102.

Ruiz-Magana, M. J., Martinez-Aguilar, R., Lucendo, E., Campillo-Davo, D., Schulze-Osthoff, K., & Ruiz-Ruiz, C. (2016). The antihypertensive drug hydralazine activates the intrinsic pathway of apoptosis and causes DNA damage in leukemic T cells. *Oncotargets, 7*, 21875–21886.

Sancataldo, G., Vetri, V., Fodera, V., Cara, G. D., Militello, V., & Leone, M. (2014). Oxidation enhances human serum albumin thermal stability and changes the routes of amyloid fibril formation. *PLoS ONE, 9*, Article# e84552.

Sekowski, S., Bitiucki, M., Ionov, M., Zdeb, M., Abdulladjanova, N., Rakhimov, R., … Zamaraeva, M. (2018). Influence of valoneoyl groups on the interactions between *Euphorbia* tannins and human serum albumin. *Journal of Luminescence, 194*, 170–178.

Seligson, N. D., Hobbs, A. L. V., Leonard, J. M., Mills, E. L., Evans, A. G., & Goorha, S. (2017). Evaluating the impact of the addition of cladribine to standard acute myeloid leukemia induction therapy. *Annals of Pharmacotherapy, 52,* 439–445.

Shahabadi, N., Akbari, A., Jamshidbeigi, M., & Fili, S. M. (2017). Interaction studies of copper complex containing food additive carmoisine dye with human serum albumin (HSA): Spectroscopic investigations. *Luminescence, 32*, 1319–1327.

Shrake, A., & Ross, P.D. (1990). Ligand-induced biphasic protein denaturation. *The Journal of Biological Chemistry, 265*, 5055–5059.

Siegel, R. L., Miller, K. D., & Jemal, A. (2018). Cancer statistics. *CA: A Cancer Journal for Clinicians, 68*, 7−30.

Stamler, J. S., Jaraki, O., Osborne, J., Simon, D. I., Keaney, J., Vita, J., … Loscalzo, J. (1992). Nitric oxide circulates in mammalian plasma primarily as an S-nitroso adduct of serum albumin. *Proceedings of the National Academy of Sciences, USA, 89*, 7674–7677.

Sudlow, G., Birkett, D. J., Wade, D. N. (1975). The characterization of two specific drug binding sites on human serum albumin. *Molecular Pharmaceutics, 11*, 824−832.

Sugio, S., Kashima, A., Mochizuki, S., Noda, M., & Kobayashi, K. (1999). Crystal structure of human serum albumin at 2.5 Å resolution. *Protein Engineering, 12*, 439–446.

Sulkowska, A. (2002). Interaction of drugs with bovine and human serum albumin. *Journal of Molecular Structure, 614*, 227–232.

Szymczyk, A., Chocholska, S., Macheta, A., Szczepanek, D., Hus, M., & Podhorecka, M. (2019). Assessment of microRNA expression in leukemic cells as predictors of sensitivity to purine nucleoside analogs, fludarabine and cladribine, in chronic lymphocytic leukemia patients. *Cancer Management and Research, 11*, 5021–5031.

Tanford, C. (1950). Preparation and properties of serum and plasma proteins. XXIII. Hydrogen ion equilibria in native and modified human serum albumins. *Journal of the American Chemical Society, 72*, 441−451.

Taupin, P. (2007). BrdU immunohistochemistry for studying adult neurogenesis: Paradigms, pitfalls, limitations, and validation. *Brain Research Reviews, 53*, 198–214.

Thompson, P. A., Tam, C. S., O'Brien, S. M., Wierda, W. G., Stingo, F., Plunkett, W., … Keating, M. J. (2016). Fludarabine, cyclophosphamide, and rituximab treatment achieves long-term disease-free survival in IGHV-mutated chronic lymphocytic leukemia. *Blood, 127*, 303–309.

Thomson, J. M., & Lamont, L. (2019). Nucleoside analogues as antibacterial agents. *Frontiers in Microbiology, 10*, 1–11.

Thor, A. D., Liu, S., Moore II, D. H., & Edgerton, S. M., (1999). Comparison of mitotic index, *in vitro* bromodeoxyuridine labeling, and MIB-1 assays to quantitate proliferation in breast cancer. *Journal of Clinical Oncology, 17*, 470–477.

Torre, L.A., Siegel, R.L., & Jemal, A. (2016). Lung cancer statistics. *Lung Cancer and Personalized Medicine, 893*, 1−19.

Trinh, A., Trumpi, K., Melo, F. D. S. E., Wang, X., de Jong, J. H., Fessler, E., … Vermeulen, L. (2017). Practical and robust identification of molecular subtypes in colorectal cancer by immunohistochemistry. *Clinical Cancer Research, 23*, 387–398.

Tsesmetzis, N., Paulin, C. B. J ., Rudd, S. G., & Herold, N. (2018). Nucleobase and nucleoside analogues: Resistance and re-sensitisation at the level of pharmacokinetics, pharmacodynamics and metabolism. *Cancers, 10*, 1–38.

Wallevik, K. (1973). Reversible denaturation of human serum albumin by pH, temperature and guanidine hydrochloride. *The Journal of Biological Chemistry, 245*, 2650−2655.

Wang, F-J., Ding, Y., Mao, Y-Y., Jing, F-Y., Zhang, Z-Y., Jiang, L-F., … Chen, K. (2014). Associations between hsa-miR-603 polymorphism, lifestyle-related factors and colorectal cancer risk. *Cancer Biomarkers, 14*, 225−231.

Wang, H., Zhou, J., He, Q., Dong, Y & Liu, Y. (2017). Azidothymidine inhibits cell growth and telomerase activity and induces DNA damage in human esophageal cancer. *Molecular Medicine Reports, 15*, 4055–4060.

Wang, Y., Wang, L. J., Zhu, M. Q., Xue, J. Y., & Li, Q. X. (2019). Comparative studies on biophysical interactions between gambogic acid and serum albumin via

multispectroscopic approaches and molecular docking. *Journal of Luminescence, 155*, 210–218.

Wigler, P. W., & Lozzio, C. B. (1972). Cytotoxic nucleoside analogs as potential anticancer agents. 5-bromodeoxyuridine 5'methykphosphonate. *Journal of Medicinal Chemistry, 15*, 1020−1024.

Yamasaki, K., Chuang, V. T., Maruyama, T., & Otagiri, M. (2013). Albumin drug interaction and its clinical implication. *Biochimica et Biophysica Acta – General Subjects, 1830*, 5435–5443.

Yasui, H., Iizuka, D., Hiraoka, W., Kuwabara, M., Matsuda, A., & Inanami, O. (2020). Nucleoside analogs as a radiosensitizer modulating DNA repair, cell cycle checkpoints, and apoptosis. *Nucleosides, Nucleotides & Nucleic Acids, 39*, 439–452.

Yeggoni, D. P., Rachamallu, A., & Subramanyam, R. (2016). Protein stability, conformational change and binding mechanism of human serum albumin upon binding of embelin and its role in disease control. *Journal of Photochemistry & Photobiology, B: Biology, 160,* 248–259.

Yuan, Q., Li, X., Lai, M-Y., Lang, J-Y., Chen, F., Zhao, R., … Ling, J. (2016). Mechanism of cerebral acupuncture for neuronal cell apoptosis via BrdU and nestin in hypoxic-ischemic brain-damaged immature rats. *European Journal of BioMedical Research, 2*, 30–36.

Zaroog, M. S., & Tayyab, S. (2012). Formation of molten globule-like state during acid denaturation of *Aspergillus niger* glucoamylase. *Process Biochemistry, 47*, 775–784.

Zhang, J., Yu, H., Sun, F-Y., Li, J., Li, D-M., & Sun, C-H. (2019). Effects of lamivudine on cell proliferation of liver cancer and expressions of HBsAG, HBeAg, and MMP-9 in patients. *European Review for Medical and Pharmacological Science, 23*, 9093–9098.

Zhang, Y. Z., Dai, J., Zhang, X. P., Yang, X., & Liu, Y. (2008). Studies of the interaction between Sudan I and bovine serum albumin by spectroscopic methods. *Journal of Molecular Structure, 888*, 152–159.

Zheng, X., Li, Z., Podariu, M. I., & Hage, D. S. (2014). Determination of rate constants and equilibrium constants for solution-phase drug-protein interactions by ultrafast affinity extraction. *Analytical Chemistry, 86*, 6454−6460.

Zhou, F-M., Huang, Y-Y., Tian, T., Li, X-Y., & Tan, Y-B. (2018). Knockdown of chloride channel-3 inhibits breast cancer growth *in vitro* and *in vivo*. *Journal of Breast Cancer, 21*, 103–111.

Zhu, H., Luo, H., Zhang, W., Shen, Z., Hu, X., & Zhu, X. (2016). Molecular mechanisms of cisplatin resistance in cervical cancer. *Drug Design, Development and Therapy, 10*, 1885–1895.

Zsila, F., Fitos, I., Bencze, G., Keri, G., & Orfi, L. (2009). Determination of human serum alpha-1 acid glycoprotein and albumin binding of various marketed and preclinical kinase inhibitors. *Current Medicinal Chemistry, 16*, 1964−1977.

LIST OF PUBLICATIONS AND PAPERS PRESENTED

List of Publications

1. **Roslan A. A.**, Mohamad S. B., & Tayyab S. (2020). Docking evaluation of the interaction between green tea active ingredient, L-theanine and human serum albumin. *National Academy Science Letters*, https://doi.org/10.1007/s40009-020-00949-5.

2. **Roslan A. A.,** Kandandapani S., Ridzwan N. F. W., Mohamad S. B., & Tayyab S. (2019). Biophysical and computational approaches to unravel the molecular interaction mechanism of bromodeoxyuridine, a proliferative marker with human serum albumin. *Monatshefte fur Chemie*, *150*, 2061−2070.

3. Kabir M. Z., **Roslan A. A.**, Ridzwan N. F. W., Mohamad S. B., & Tayyab S. (2019). Biomolecular interaction of a platelet aggregation inhibitor, 3, 4-methylenedioxy-β- nitrostyrene with human serum albumin: Multi-spectral and computational characterization. *Journal of Biomolecular Structure and Dynamics*, *15*, 1−11.

4. **Roslan A. A.**, Mohamad S. B., & Tayyab S. (2019). Exploring ligand−protein interaction: A laboratory exercise on herbicide binding to plasma transport protein. *Biochemistry and Molecular Biology Education*, *47*, 156−160.

Paper Presented

1. **Roslan A. A.,** Kandandapani S., Ridzwan N. F. W., Mohamad S. B., & Tayyab S. (2019). *Biophysical and computational characterization of the interaction between bromodeoxyuridine and human serum albumin.* Paper presented at the 27th FAOBMB & 44th MSBMB Conference, 19 - 22 August 2019, Kuala Lumpur, Malaysia.